

**JIMMA UNIVERSITY**  
**SCHOOL OF GRADUATE STUDIES**  
**COLLEGE OF NATURAL SCIENCES**  
**DEPARTMENT OF CHEMISTRY**



**M.Sc THESIS**

**ON**

**SYNTHESIS OF Ag-ZnO NANOCOMPOSITE USING *PSIDIUM GUAJAVA* LEAF  
EXTRACT AND EVALUATION OF ITS PHOTOCATALYTIC ACTIVITY**

**BY:**

**DEREJE DADI**

**ADVISORS: GUTA GONFA (PhD)**


**BIRKINESH GIRMA (M. Sc)**

**FEBRUARY, 2021**

**JIMMA, ETHIOPIA**

**SCHOOL OF GRADUATE STUDIES**  
**JIMMA UNIVERSITY**  
**COLLEGE OF NATURAL SCIENCES**  
**MSc THESIS APPROVAL SHEET**

We, the undersigned, member of the Board of Examiners of the final open defense by **Dereje Dadi Tulu** have read and evaluated his thesis entitled “**Synthesis of Ag-ZnO Nanocomposite Using *Psidium Guajava* Leaf Extract and Evaluation of its Photocatalytic Activity**” and examined the candidate. This is therefore to certify that the thesis has been accepted in partial fulfillment of the requirements for the degree Master of Science in **Chemistry (Inorganic)**.

<u>Mr. Gebru Gebretsadik (PhD Cand.)</u> Name of the Chairperson	_____ Signature	_____ Date
<u>Dr. Guta Gonfa (Assi. Prof.)</u> Name of Major Advisor	_____ Signature	_____ Date
<u>Mrs. Birkinesh Girma (Lect.)</u> Name of Co-Advisor	_____ Signature	_____ Date
<u>Dr. Negera Abdissa (Assoc. Prof.)</u> Name of the Internal Examiner	_____ Signature	_____ Date
<u>Dr. Raji Feyisa (Assi. Prof.)</u> Name of the External Examiner	 _____ Signature	_____ Date

## Table of Contents

Contents	Page
Table of Contents.....	i
Acknowledgment.....	iv
List of Figures.....	v
List of Schemes.....	vi
Abbreviations and Acronyms.....	vii
Abstract.....	viii
1. Introduction.....	1
1.1. Background of the Study.....	1
1.2. Statement of the Problem.....	3
1.3. Objectives.....	4
1.3.1. General Objective.....	4
1.3.2. Specific Objectives.....	4
1.4. Significance of the Study.....	4
2. Review of Related Literatures.....	5
2.1. Environmental Pollutions Due to Dye Effluents and Human Health Issue.....	5
2.2. Nanomaterials, Nanoscience and Nanotechnology.....	6
2.3. Methods for Synthesis of Ag Doped ZnO Nanocomposite.....	7
2.4. Botanical Information of <i>Psidium Guajava</i> Plants and its Medicinal Values.....	9
2.5. Preliminary Phytochemical Analysis of the <i>Guava</i> Leaf Extract.....	10
2.6. Characterizations of Metal Doped Metallic Oxide Nanoparticles.....	11
2.6.1. Ultraviolet-Visible (UV–Vis) Spectroscopy.....	11
2.6.2. Fourier Transformed Infrared Spectroscopy (FT-IR).....	12
2.6.3. Powder X-ray Diffraction (XRD) Analysis.....	12

2.7. Applications of Plant Mediated Ag Doped ZnO Nanocomposite.....	13
2.7.1. Photocatalytic Degradation of Dyes Using Ag Doped ZnO Nanocomposite .....	13
3. Materials and Methods.....	17
3.1. Experimental Site and Period.....	17
3.2. Materials and Chemicals .....	17
3.3. Apparatus .....	17
3.4. Scientific Instruments.....	18
3.5. Sample Collection and Preparation .....	18
3.6. Preliminary Phytochemical Screening of the Plant Extract .....	18
3.6.1. Test for phenols .....	18
3.6.2. Test for Alkaloids .....	19
3.6.3. Test for Saponins .....	19
3.6.4. Test for Flavonoids.....	19
3.6.5. Test for Tannins.....	19
3.7. Optimization of Some Parameters.....	19
3.8. Synthesis of ZnO Nanoparticles Using <i>Guava</i> Leaf Extract.....	19
3.9. Synthesis of Ag-ZnO NCs Using <i>Guava</i> Leaf Extract .....	20
3.10. Characterizations of the Synthesized Ag-ZnO NCs.....	20
3.11. Photocatalytic Activity.....	20
3.11.1. Optimum Experimental Conditions.....	20
3.11.2. Photocatalytic Degradation of Methylene Blue Dye.....	20
3.11.3. Recyclability of the Photocatalyst .....	21
4. Results and Discussion .....	22

4.1. Preliminary Phytochemical Screening of the <i>Guava</i> Leaf Extract .....	22
4.2. Optimization of Important Parameters.....	23
4.3. UV-Vis Absorption Spectral Analysis .....	24
4.4. FT-IR Spectroscopic Study .....	26
4.5. XRD Analysis .....	28
4.6. Optimization of Photocatalytic Parameters.....	29
4.6.1. Effect of Ag-ZnO NCs Catalyst Dose .....	29
4.6.2. Effect of Initial Dye Concentration .....	30
4.6.3. Effect of pH and Point of Zero Charge.....	31
4.6.4. Effect of Irradiation Time.....	33
4.7. Photocatalytic Degradation Activity .....	34
4.8. Re-usability of the Photocatalyst.....	37
5. Conclusions and Recommendations .....	39
5.1. Conclusions .....	39
5.2. Recommendations .....	39
References.....	40
Appendix A.....	51
Appendix B .....	52
Appendix C .....	53
Appendix D.....	54
Appendix E .....	55

## **Acknowledgment**

I am grateful to my advisor Dr. Guta Gonfa for his scientific guidance, continuous support and motivation during the entire period of this work, beginning from proposal development up to the completion of the thesis. I also grateful to my co-advisor Birkinesh Girma (M.Sc) for her advises and comment throughout this work. Next, I would like to thank the entire staff members of chemistry department, University of Jimma, and my classmates and friends who shared me their experiences, valuable information and materials and for their tireless efforts and working closely with me. I would also grateful to department of chemistry, Jimma University for the sponsorship.

Finally, I would thankful to Material Engineering department Institute of Technology, Jimma University for their support in analyzing the FT-IR and XRD of the samples.

## List of Figures

Figure 1: <i>Psidium Guajava</i> L.....	3
Figure 2: Different Methods for Synthesizing of Nanoparticles. ....	7
Figure 3: Structures of Some Isolated Compounds from <i>P. Guajava</i> Leaves. ....	10
Figure 4: Chemical Structures of Some Secondary Metabolites. ....	11
Figure 9: FT-IR Spectra of the Extract (a), ZnO NPs (b) and Ag-ZnO NCs (c). ....	27
Figure 10: XRD Pattern of Ag-ZnO NCs (a) and ZnO NPs (b). ....	29
Figure 11: Effects of Ag-ZnO Dose on MB Photodegradation. ....	30
Figure 12: Effects of MB Dye Concentration on Photodegradation.....	31
Figure 13: Determination of pH at Point of Zero Charge. ....	32
Figure 14: pH Effects on Percent Degradation of MB Dye.....	32
Figure 15: Effects of Irradiation Time on Photodegradation of MB. ....	34
Figure 16: UV-Vis of MB Catalyzed by Ag-ZnO NCs (a) and Uncatalyzed MB (b).....	35
Figure 17: Photocatalytic Percent Degradation Efficiency of MB. ....	37
Figure 18: Cycling Times of the Photodegrading MB Applying ZnO-Ag NCs Catalyst.....	37

## **List of Schemes**

Scheme 1: Simple Model Mechanism of Green Synthesis of Ag-ZnO NCs.....	9
Scheme 2: The Proposed Conduction and Valence Band Diagram.....	14
Scheme 3: Proposed Photocatalytic Reaction Mechanism.....	15
Scheme 4: The Degradation Pathways of MB Reacting with Photocatalytic Oxidation.....	16



## Abbreviations and Acronyms

CB	Conduction Band
EDX	Energy Dispersive X-Ray Spectrometer
FT-IR	Fourier Transformed Infrared
JCPDS	Joint Committee on Powder Diffraction Standards
MB	Methylene Blue
NCs	Nanocomposites
NPs	Nanoparticles
pHpzc	pH at Point of Zero Charge
PXRD	Powder X-ray Diffraction Analysis
PZC	Point of Zero Charge
SEM	Scanning Electron Microscopy
SPR	Surface Plasmon Resonance
TEM	Transmission Electron Microscopy
TGA	Thermogravimetric Analysis
UK	United Kingdom
USA	United States of America
UV–Vis	Ultraviolet-Visible
VB	Valence Band

## Abstract

The increase of environmental pollutions from industry due to organic dye effluents initiated the researcher to design a nanomaterial with a target of photocatalytic degradation capacity. So, the main objective of this thesis was to synthesize Ag-ZnO NCs using *Psidium guajava* leaf extracts and evaluate its photocatalytic activity. A simple, ecofriendly, inexpensive, short-time consumer and biocompatibility approach was developed for the synthesis of Ag-ZnO NCs using *P. guajava* leaf extract without employing any chemical stabilizer. The phytochemical screening analysis of the plant extract confirmed the presence of alkaloids, flavonoids, phenols, tannins and saponins. The synthesized crystalline nanoparticles were characterized by UV-Vis, FT-IR and XRD. The UV-Vis absorbance peak for ZnO and Ag-ZnO were 374 and 375 nm with band gap of 3.02 and 2.86 eV respectively. The FT-IR result showed the presence of functional groups in the leaf extract and prepared nanoparticles. Furthermore, a good coordination of functional groups with the synthesized NPs were observed as it displayed red-shift of absorbance peaks. The XRD data revealed that the average crystalline size of ZnO and Ag-ZnO were 22 and 26 nm, respectively. Photocatalytic activity of Ag-ZnO NCs was performed under natural sunlight using methylene blue as organic dye pollutant. The dye was entirely decolorized and degraded by more than 98% after irradiation for 120 min. In contrast, the solar light catalyzed dye was not decolorized still it was irradiated upto 200 min. Therefore, the present study provided that the Ag doped ZnO nanocomposites may have good applications and high-efficiency of photocatalytic activity.

**Keywords:** *Psidium guajava* leaf extracts, Ag-ZnO Nanocomposites, Photocatalytic degradation, Green synthesis, Phytochemical screening.

# 1. Introduction

## 1.1. Background of the Study

Evidently, increasing of the world's population is leading to unexpected urbanizations and industrializations in which it can cause environmental pollutions. Environmental and water contamination has been a major issue due to the discharge of organic dye pollutants into the water supply system from major industries such as paper, plastic, pharmaceutical, textiles, cosmetics, food, leather, medicine and many other industries [1]. About 20% of dyes such as methylene blue, phenols and other phenolic dyes are released to the environment during manufacturing processes. The presence, accumulation and stability of these dyes in the environment and water body can cause severe effects on humans, animals, plants, the nature of water and inhibit the sunlight penetration and reduce the normal photosynthetic reaction since they are toxic, carcinogenic and mutagenic in nature [1-4]. This societal issue was initiated the researcher to design a safe and cheap plant extract mediated nanomaterial with better potential photocatalytic activity.

Nowadays, nanotechnology is an interesting science due to its wide applications to a variety of industrial and purification processes [5]. Nanotechnology helps in reducing the particle size of materials as an efficient and reliable tool for improving their biocompatibility (well-matched) and can globally change the view regarding science [6]. Nanoparticles (NPs) are a key product of nanotechnology having a unit dimension in the range of 1–100 nm [7]. Due to their vast potential applications in various fields, the synthesis and engineering of metal doped metallic oxide nanoparticles find great scope in the present era of urbanization and industrialization as metal oxides is of prime importance for environmentally sustainable manner [4, 8, 9].

In order to synthesize metal doped metallic oxide NPs, the biological routes such as plant, fungi, bacteria and other natural sources has gained more attention than physical and chemical methods. The chemical syntheses methods of nanomaterials are quite expensive and involve hazardous chemicals that can cause carcinogenicity, general toxicity, and there is a need to develop rapid procedure for synthesis of nanomaterials using plant based bioactive compounds *via* green methods. Using plants for nanoparticle synthesis might be advantageous over other biological

processes because it eliminates the elaborate process of maintaining cell cultures, can be suitably scaled up for large-scale nanoparticle synthesis, safety, nontoxic, ecofriendly, protocols with non-toxic byproducts, gentle reaction condition requirements, the use of natural capping and reducing agents, cost effective, very low cytotoxicity, greater film forming capacity and usage in a wide array of biomedical applications [7, 10-12]. Plants are abundant, inexpensive, and rich in different bioactive chemicals heavily utilized for the purpose of reducing and capping agents that are important in photocatalytic active nanomaterials synthesis [10, 11].

Among metal doped metallic oxide NPs, Ag-ZnO nanocomposites (NCs) have concerned large attention because Zinc oxide (ZnO) has more chemical stability, low cost, large surface area. ZnO has several applications that include usage in solar cells, photocatalytic activity, electrochemical capacitors and batteries, various optoelectronic devices and thin film, electronics, photo electronics, and gas sensors due to its wide band gap (3.37 eV at room temperature 300 K), as Ag nanomaterials illustrate some distinctive properties in biological and chemical sensing and high electrical conductivity. The optical direct band gap of Ag NPs is 3.4 eV. Recently, Ag ions have gained more attention in several research studies due to their newly discovered effects on the evolution of antibacterial activity and efficiency of photocatalytic activity of semiconductor [12-14].

*Psidium guajava* L. (*Guava*) is a medicinal plant in family Myrtaceae and is one of the most important economic fruits in tropical and subtropical areas of the worldwide [15-18]. The *Guava* leaves own many biological effects that can support the good health of human being such as hepatoprotective effect, antioxidant, anti-inflammatory, anticough, antidiarrheal, antiamebic, antibacterial, and anti-hyperglycemic as well as anti-hyperlipidemic effects [15, 16]. Some of the main constituents of *Guava* are in the groups of vitamins, tannins, phenolic compounds, flavonoids, sesquiterpene alcohols and triterpenoid acids (fig. 1) [15, 16].



Figure 1: *Psidium Guajava* L.

Currently, *P. guajava* has been explored in terms of landscaping and molecular characterization; however, no reports are available for utilization of it in the greener synthesis of metal doped metallic oxide nanoparticles. Due to the richness in phytochemicals it produces, the *Guava* leaf was selected as a potential candidate for synthesis of Ag-ZnO nanocomposite.

## 1.2. Statement of the Problem

The synthesis of nanoparticles using physicochemical methods have been remain expensive, use of toxic, hazardous and non-ecofriendly chemicals, use of high pressure, temperature and energy, required complication operative conditions [19]. The need to develop cost effective and ecofriendly method for nanoparticle synthesis attracted the attention of researchers to exploit the biological entities for Ag doped ZnO nanoparticles by utilization of phytochemicals from plant extracts. The studies focused on synthesis of Ag doped ZnO nanoparticles using *P. guajava* leaf extract are scarce. Photocatalytic effect of ZnO and Ag is obvious, but only a few studies were presented in the case of the potency of Ag doped ZnO [12].

Generally, this research was designed to answer the following questions:

- What is the efficiency of photocatalytic degradation activity of the synthesized Ag-ZnO nanocomposites?

- Does the photocatalytic applications of the synthesized Ag-ZnO nanocomposites consistent with the reported values in related literatures?

### **1.3. Objectives**

#### **1.3.1. General Objective**

- The main objective of this study was to synthesize Ag-ZnO nanocomposites using *Psidium guajava* leaf extract for photocatalytic activity.

#### **1.3.2. Specific Objectives**

- To synthesize *P. guajava* leaf extract supported ZnO NPs and Ag-ZnO NCs.
- To characterize the synthesized ZnO NPs and Ag-ZnO NCs using UV-Vis spectroscopy, FT-IR and XRD.
- To evaluate the photocatalytic activity of the synthesized Ag-ZnO NCs using methylene blue.

### **1.4. Significance of the Study**

Synthesizing of ZnO NPs and Ag-ZnO NCs materials have been considered for numerous applications ranging from a new generation of solar cells to bio- and chemo-sensors [20-22].

Moreover, the findings of this research could be used for:

- Upgrading the knowledge about the Ag-ZnO NCs regarding its photocatalytic activity.
- Providing further awareness for researchers about the application of the green synthesized Ag-ZnO NCs.

## 2. Review of Related Literatures

### 2.1. Environmental Pollutions Due to Dye Effluents and Human Health Issue

We are in the era of urbanization and industrialization, which requires different domains of electronics, energy storage devices, ecological remediation, microbial inhibition, medical implants and optical appliances [4]. About 10,000 different commercial organic dyes and pigments exist and more than  $7 \times 10^5$  tons are produced per year over the worldwide and have been used in many industries such as textiles, printing, leather, pulp, food and plastics, etc. Approximately, 10-15% of these dyes are released through effluents after dyeing processes and can cause the environmental pollution [22]. As these compounds are toxic and carcinogenic in nature, their impact on the environment and human health is a major concern. Furthermore, these dyes impart color to aqueous body by blocking the penetration of sunlight and dissolution of oxygen [23].

Thus, the synthesis of metal doped metallic oxide nanoparticles finds a great scope for their interesting applications in removing these dyes [4]. Doping of ZnO with transition metals like Ag, Pd, Pt and Au may prove beneficial [24]. However, the photocatalytic activity of ZnO is limited to the UV region and can only absorb UV light with wavelengths below 387 nm. The fast recombination rate of the photogenerated electron-hole pairs also hinders the industrial application of this semiconductor [24].

Considerable efforts have been made to modify ZnO nanoparticles in order to improve its catalytic efficiency in the visible-light region. The advantages of photocatalysts modifications are to delay electron-hole recombination, to broaden the absorption spectrum, to facilitate some specific reactions on the surface of catalysts and to improve photostability [24].

Nowaday, there is a growing need to develop the ecofriendly techniques for nanoparticle synthesis in order to increase its application in the medical and environmental platforms which can avoid the use of hazardous chemicals and solvents [25-27].

Ag-ZnO nanomaterials are very important in developing sustainable technologies for the future, humanity and the environment since they are well known for both antimicrobial and pro-healing properties [25, 26, 28]. Synthesis of nanomaterials through different physical and chemical

routes possess an inherent damage to the environment, economy, need for high temperature and pressure, expensive equipment, toxic reagents, longer reaction time, and needs manual effort. In contrary, biological entities (i.e. bacteria, fungi, and plants) can be used as the bio factories for NP synthesis since it is a simple and ecofriendly method [11, 25, 26, 28].

Previously conducted researches showed that plant mediated synthesis of Ag-ZnO nanocomposites as a green approach has greater standing than physical and chemical techniques. The plant extracts supported Ag-ZnO nanocomposites reasonable the evaluation of photocatalytic activity [12].

## **2.2. Nanomaterials, Nanoscience and Nanotechnology**

Nanomaterial is a substance having a nano scale dimension of 1-100 nm. The unit of nanometer derives its prefix nano from a Greek word meaning “dwarf” or “extremely small.” One nanometer span 3-5 atoms lined up in a row. By comparison, the diameter of a human hair is about 5 orders of magnitude larger than a nanoscale particle. Nanomaterial exhibits unique physical and chemical (optical, magnetic, electrical etc) properties absent in both the molecular and bulk solid state [19, 29]. Nanomaterials can be metals, ceramics, polymeric, or composite materials [30]. Their unique properties lead it to have a great application potential in the field of nano technology, electronics, medicine, and other fields by displaying different physical and chemical characteristics from normal chemicals (i.e., silver nano, carbon nanotube, fullerene, photocatalyst, carbon nano, silica). Many components of electronic and optical devices used for information processing, storage, and display are being improved through the development of new solid-state materials nanotechnology [31].

Nanomaterials can be nanoscale in one dimension (eg. Surface films), two dimensions (eg. strands or fibers), or three dimensions (eg. particles). They can exist in single, fused, aggregated or agglomerated forms with spherical, tubular, and irregular shapes [31].

Nanotechnology is the collection of procedures for manipulating matter in scale in order to build nanosized entities for useful purposes. Thus, nanomaterials are cornerstones of nanoscience and nanotechnology which taken to be as solid material and exhibits novel properties related to its scale [29]. Nanotechnology is a promising science with wide applications from cosmetics, food products, clothing, and household appliances to fuel catalyst, disease treatment, and renewable



energies; And is also being applied to a variety of industrial and purification processes including construction materials, nanomachining of nanowires, nanorods, graphene, water filtration, and wastewater treatment, energy storage, automotive parts, thin-film electronics, coatings, and so forth [5].

### 2.3. Methods for Synthesis of Ag Doped ZnO Nanocomposite

There are three basic fabrication techniques of nanoscale entities, namely physical, chemical and biological synthesis approaches. Physical synthesis process basically depends upon the instruments used in the experiment. Electron beam lithography, arc discharge and ball milling are among methods used for synthesis of nanomaterials [28]. Chemical method of synthesizing NPs depends on chemicals, reducing and capping agents along with an optimum condition of temperature and pressure. Electrochemical, microemulsion, ozonation etc. are some of chemical synthesizing techniques. The biological approach for NPs synthesis is ecological agreeable and is called “Green synthesis” due to its non-toxic, save reagents, not perilous to any living beings. Fig. 2 shows that different synthesizing methods of nanoparticles [28, 29, 32, 33].

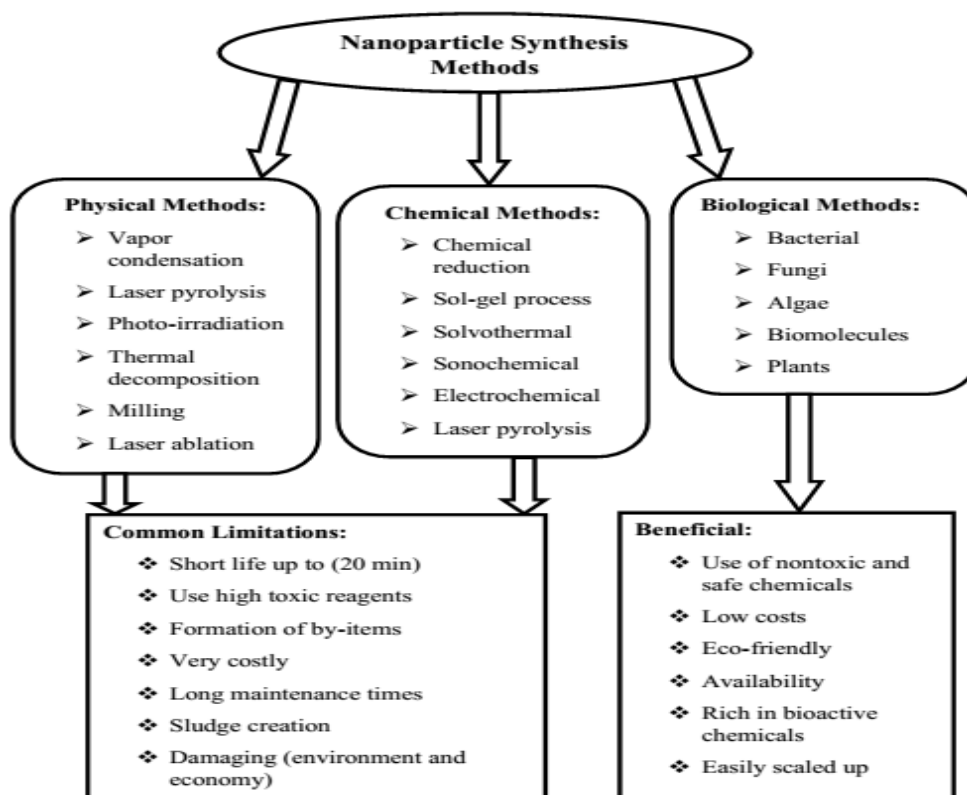
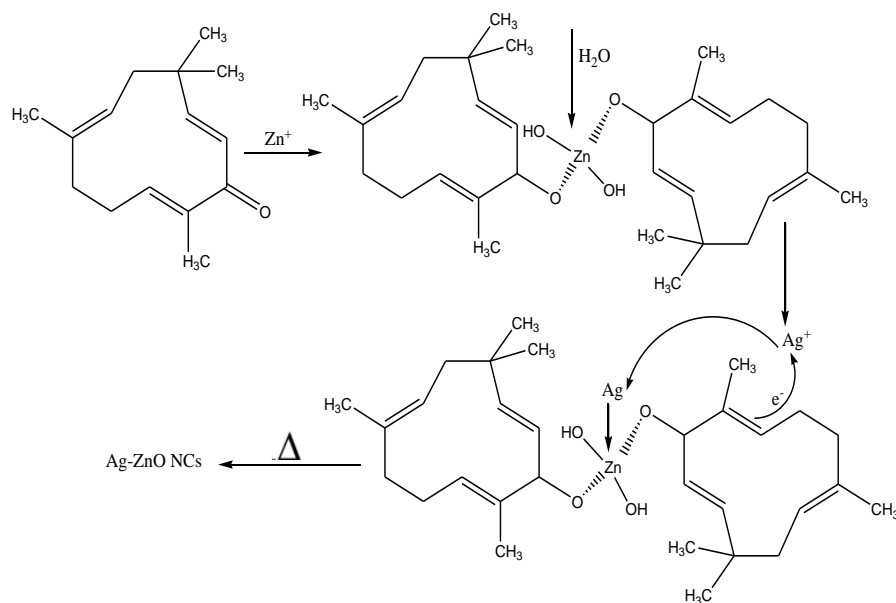


Figure 2: Different Methods for Synthesizing of Nanoparticles.

Zinc oxide nanomaterials have been synthesized by different methods such as the co-precipitation, sol-gel, combustion, hydrothermal, and thermal decomposition, depending on the desired structure [34]. Similarly, several synthetic methods are available for the synthesis of nanoscale silver such as chemical, photochemical, electrochemical, microemulsion, and microwave. Modifying of ZnO NPs could be utilized as a base material for applications of semiconductors, gas sensors, and antimicrobial and photocatalysis activity [34, 35]. Ag doped ZnO nanoparticles have been fabricated by variety of physicochemical processes e.g. sol-gel, oxidative reactions, thermo-evaporative, co-precipitative, vapor deposition through chemical method and sonochemical reactions [4]. Most of these methods involve the use of toxic chemicals and severe reaction conditions which lead to chemical toxicity and environmental pollution so that the increasing focus on green chemistry have augmented the importance of biosynthesis method [35]. Green chemistry explained the biogenic route for Ag doped ZnO nanoparticles by utilization of phytochemicals from plants [4, 36].

Biological processes such as bacteria, fungi, yeast, enzymes, plants, algae, collagen, macromolecules and amino acid sequences has been proposed as a simple alternative to physicochemical methods for nanoparticle synthesis due to their ease, low cost, nontoxic and an ecofriendly nature [35, 37, 38]. Plants are now acquiring high interest over other biological processes because they constitute bioactive polyphenols, alkaloids, tannins, terpenoids, flavonoids, saponins, proteins, sugars and phenolic acids, which are made-up to have an important role in primarily reducing the metallic ions and then stabilizing them. Plant parts, such as root, leaf, latex, seed and stem, are widely being used for metal-based nanoparticle synthesis [11, 25, 26, 28, 35, 37, 38]. Scheme 1 illustrated the main probable mechanism of biosynthesis of Ag-ZnO NCs through plant extracts [12, 39].



Scheme 1: Simple Model Mechanism of Green Synthesis of Ag-ZnO NCs.

#### 2.4. Botanical Information of *Psidium Guajava* Plants and its Medicinal Values

*Psidium guajava* L., commonly known as *Guava*, is belongs to the family of Myrtaceae [16, 40]. This family plants are composed of 140 genera and 3400 species distributed largely in the tropical and subtropical region of the world [17].

The fruit of this plant is commonly used as diet and traditional medicine, and can be made available in all seasons and everywhere [17, 18]. *Guava* plants have many medicinal uses, like antifilarial, antidiarrheal, anticough, antiamebic, antispasmodic, antibacterial, antimicrobial and antioxidant activity, antiulcer, etc. [16-18]. The species is highly biologically active presenting hepatoprotective, antiallergic, antigenotoxic, cardioactive, anti-inflammatory, antihyperglycemic, anti-hyperlipidemic effects and is also known by its antimutagenic potential [40].

Carotenoids, triterpenoids, polyphenolic compounds as flavonoids and tannins are the main phytochemicals characterized in *Guava* leaves and fruits [17, 41]. The leaves of the plant also contain chemical compounds such as steroids, phenolic acids (gallic acid) and essential oils (bisabolene, cineol) [40], vitamins, fiber and fatty acids, glycosides and saponins [41, 42]. Guavenoic acid, Quercetin acid and Guavanoic acid are some of the isolated compounds from leaves of *P.guajava*. They are rich in hydroxyl (OH) and carbonyl (C=O) functional groups accountable for reducing and stabilizing agents in nanoparticles synthesis [42].

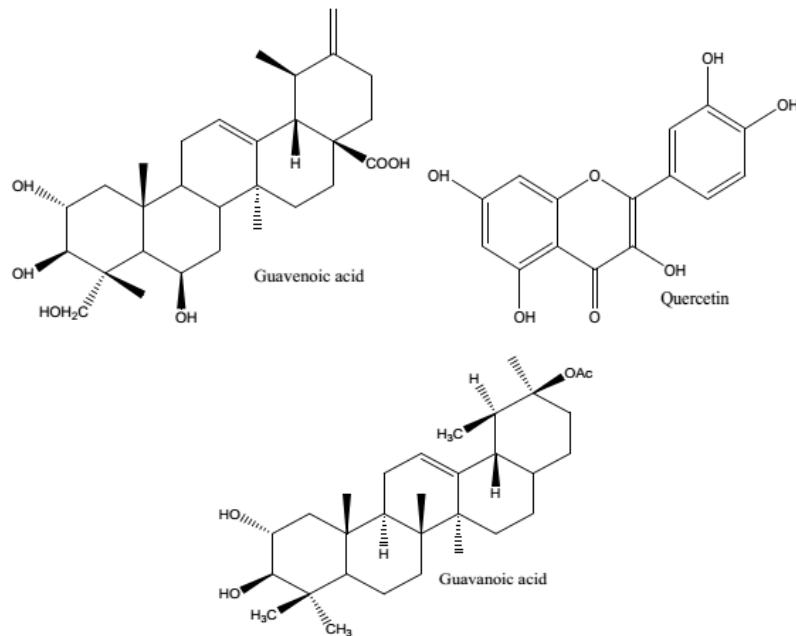


Figure 3: Structures of Some Isolated Compounds from *P. Guajava* Leaves.

### 2.5. Preliminary Phytochemical Analysis of the *Guava* Leaf Extract

Phytochemical is chemical compounds that occur naturally in plants and can be derived from any part of the plant like bark, leaves, fruits, flowers, roots, seeds. Plants are rich in a variety of phytochemicals constituents including tannins, terpenoids, alkaloids, saponins, phenols, flavonoids etc. [43-46]. Qualitative phytochemical analysis of the plant extract was performed using the standard methods described in the literatures for determining the presence of different class of compounds including alkaloids (Mayer's, Wagner's, Dragendroff's reagents), flavonoids (Shinoda alkaline reagent), phenolic compounds (lead acetate, alkaline reagent test), triterpenes (Lieberman Burchard test), saponins (foam test), and tannins (gelatin) [20, 43-46].

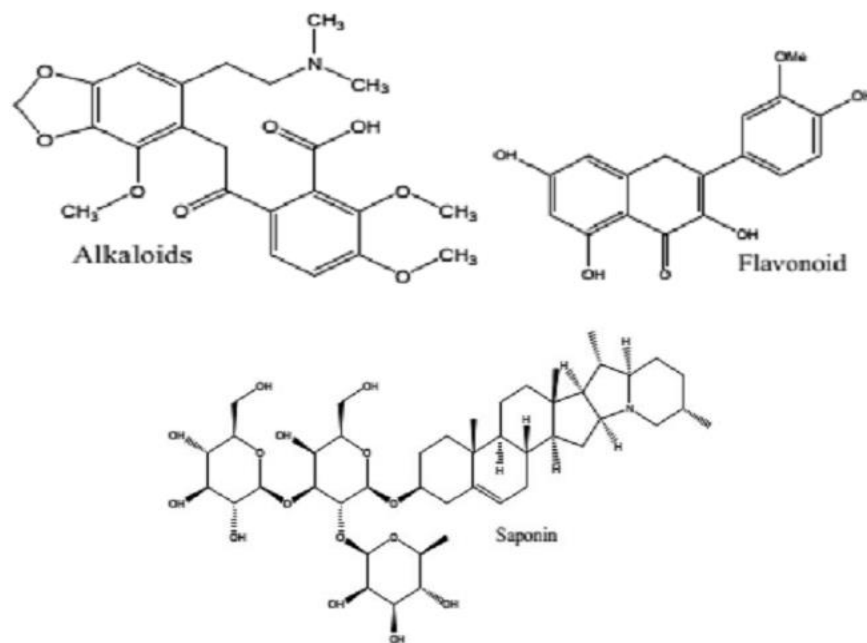


Figure 4: Chemical Structures of Some Secondary Metabolites.

## 2.6. Characterizations of Metal Doped Metallic Oxide Nanoparticles

The great advances made in nanosciences and nanotechnology would not have occurred without the ability to characterize the nanoscale structural, chemical, and physical properties of materials. Moreover, the direct observation of nanostructure allows meaningful relationships between processing and properties to be made [29].

### 2.6.1. Ultraviolet-Visible (UV-Vis) Spectroscopy

UV-Vis spectroscopy is the valuable technique commonly used to identify the structural characterization, formation and stability of metal nanoparticles in aqueous solution by analyzing the unique optical properties and optical band gap which depends on the size and the shape of the nanoparticles between 200 nm to 800 nm. It is well recognized that the optical absorption peak of metal nanoparticles is dominated by surface plasmon resonances (SPRs) that shift to longer wavelengths with increasing particle size due to the capping agent. The SPR mainly depended upon the size and shape of nanoparticles [9, 10, 12, 30, 47].

The metal ion reduction can be confirmed by the apparent change in the color of the reaction mixture as characterized by UV-vis spectrum. Indeed, no color transformation can be noticed in the absence of plant extract, under a similar set of situations. The formation of NPs was further

confirmed by UV-vis spectral study, which is a reliable technique to monitor the progress of the reaction during the reduction of metal ions [48]. The UV-vis spectrum of green synthesized NPs using plant leaf extract can show the significant changes in the absorbance maxima due to surface plasmon resonance demonstrating the formation of NPs [49]. The band gap energy of photocatalysts can be determined based on its adsorption edge wavelength according to equation  $E_g = 1239/\lambda$  [12, 50].

### **2.6.2. Fourier Transformed Infrared Spectroscopy (FT-IR)**

FT-IR spectroscopy is used to identify the possible functional groups of the active components present in the extracts or on the surface of NPs that are responsible for reducing, capping and stabilizing of being synthesized nanoparticles. The functional groups are identified in the ranges of  $4000-400\text{ cm}^{-1}$ . The FT-IR peaks attributed to stretching and bending vibrations is identified and assigned the different functional groups present in the leaf extract and as well as in the nanoparticles [16, 34, 44, 47, 51].

The FT-IR spectrum of plant extract exhibits several absorption peaks at different locations, and which are associated with the several oxygen-comprising functional groups [48]. After the reaction, a majority of the peaks exist in the FT-IR spectrum of NPs, but they decreased in intensity and also showed with few marginal shifts into lower wavenumber. Consequently, the occurrence of these peaks evidently indicates the dual role of the plant extract, both as a green reducing agent and as a stabilizing agent [48, 52].

### **2.6.3. Powder X-ray Diffraction (XRD) Analysis**

The XRD spectra are used to confirm the crystalline nature, the structure, phase purity and composition of synthesized nanoparticles. The X-ray diffraction pattern of nanoparticles can be confirmed by the characteristic peak observed in XRD image. The data are collected in the  $2\theta$  range [34, 53]. The average crystallite size of the NPs can be calculated using Debye-Scherrer's equation [50].

$$D = \frac{0.89\lambda}{\beta \cos\theta}$$

Where,  $D$  = average crystallite size,  $\lambda$  = wavelength of X-ray beam (1.5406Å),  $\theta$  = scattering angle in degree, and  $\beta$  is the full width half maximum of plane (XRD peak).

## **2.7. Applications of Plant Mediated Ag Doped ZnO Nanocomposite**

The main areas of application of photocatalysts in industry are: ecological purification of industrial wastewaters and industrial gas waste, hydrogen production, CO production in methanol industry, in solar energy, water purification from organic pollutants; organic impurities are subjected to complete destruction, forming mineral acids and compounds which are safe for the environment [54].

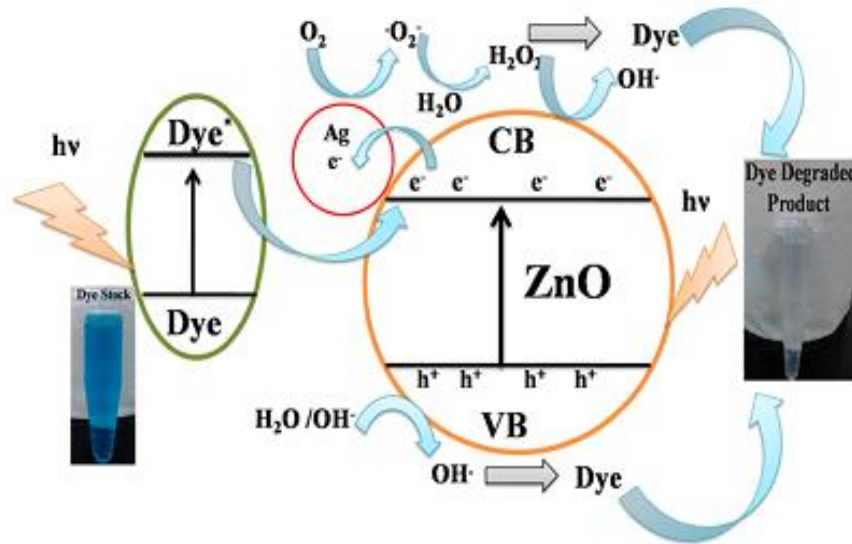
Because of the remarkable properties (antimicrobial, thermal, optical and electrical), Ag NPs used in airborne products (sprays and disinfectants), consumer products used in our daily life (toothpastes, deodorants, shampoos, water purification, air filter and kitchen utensils) and textile industry (synthetic dyes used in wet processing) [37]. Also, ZnO NPs have wide applications including catalysts, sensors and solar cells. To enhance the performances of bare ZnO, hybridization with Ag metal has extensively been employed. For Ag doped ZnO, it is generally believed that the surface plasmon resonance (SPR) of Ag enhances visible light absorption to increase the photocatalytic activity [55, 56].

The plant material containing bioactive substances are positively affecting the humans and also improve the health condition as well as good environment. Production of nanomaterials using living organisms of plant-based materials and other biodegradable polymers are an active part of bio-nanotechnology. The biosynthesized nanoparticles, such as Ag, Au, Pt, are widely used in biomedicine, pharmaceuticals, bio-labelling, food packaging, cosmetics, catalysis and sensory applications [37].

### **2.7.1. Photocatalytic Degradation of Dyes Using Ag Doped ZnO Nanocomposite**

As one of the most promising semiconductor photocatalysts, ZnO has a wide band-gap energy, high oxidative capacity, physical and chemical stability, nontoxicity, low cost, and easily available so that a great attention in research and industries is given due to its good potential photocatalyst effect [24, 57]. The common process for photocatalytic degradation of organic matters usually involves the following steps [12, 57-59]:

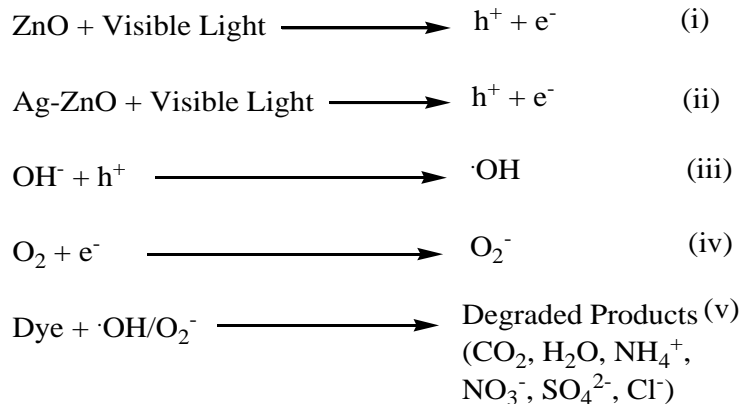
- (i) An electron is excited to the conduction band (CB) when the energy of a photon is equal to or higher than the band gap ( $E_g$ ) of the semiconductor, leaving a positive hole in the valance band (VB);
- (ii) The photoinduced electrons and holes can be trapped by oxygen and surface hydroxyl, with the generation of hydroxyl radicals known as the elementary oxidizing species;
- (iii) The hydroxyl radicals mineralize the adsorbed organic substances.



Scheme 2: The Proposed Conduction and Valence Band Diagram.

The super oxide anion radical ( $O_2^-$ ) produced by photoexcited electron has the ability to generate more  $H_2O_2$  and  $OH\cdot$  radicals. The oxygen vacancies act as traps for photoinduced electrons which further restrain temporarily the recombination of photogenerated electron-hole. The photogenerated electron further attack the dissolved oxygen and create surface bound superoxide anion along with hydroxyl ion which is further responsible for dye mineralization for photocatalytic reaction. The generated  $OH\cdot$  radical is enough to break the different bond in the dye (C-N, C=N, C-S, N=N, C-C etc) and lead to covert dye into  $CO_2$ ,  $H_2O$  and inorganic ions ( $NH_4^+$ ,  $NO_3^-$ ,  $SO_4^{2-}$ ,  $Cl^-$ ) [59].



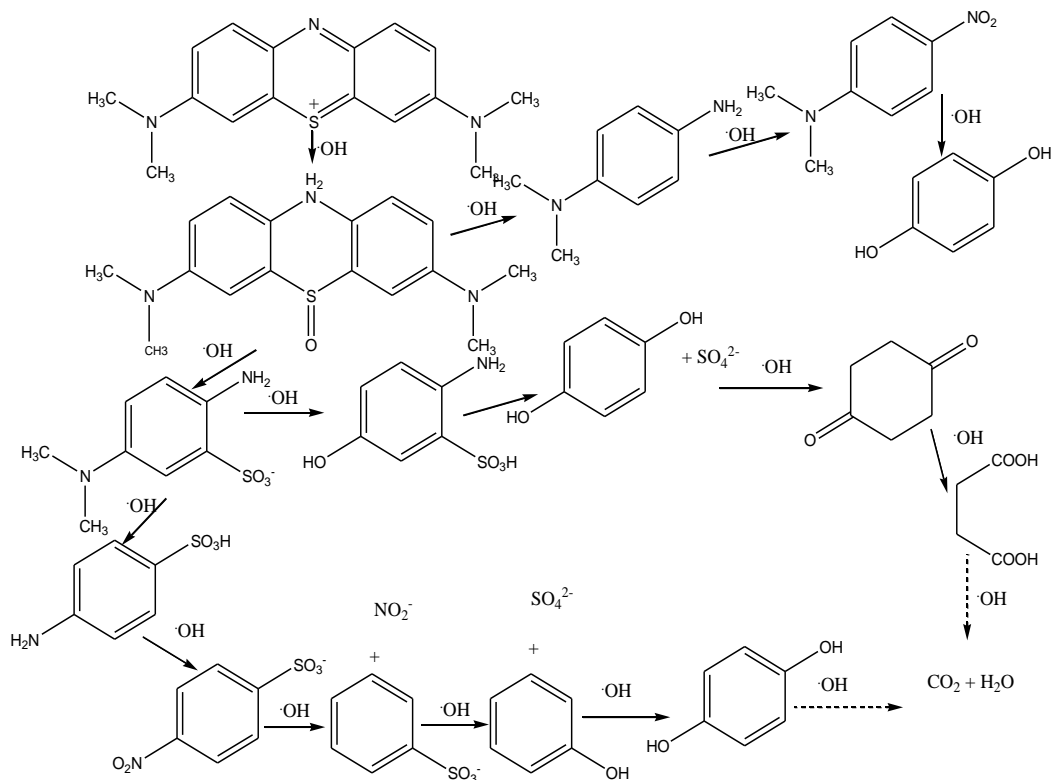


Scheme 3: Proposed Photocatalytic Reaction Mechanism.

Many organic dyestuffs are harmful to human being, animals, and microorganisms and hence it is mandatory to remove the spent dyes before its release into natural water bodies. Various dye removal process has been used, including coagulation, chemical oxidation, membrane separation, electrochemical process, biological treatment and adsorption techniques [22]. In photocatalytic applications, nanoparticles are used to remove numerous azo dyes, such as methylene blue, methyl orange, rhodamine B, and methyl red [36].

Because of the fact that the optical and electrical properties of semiconductors modify largely with the grain size, size distribution and morphology, nanosized ZnO has attracted a lot of attention in electronic and optical devices, gas sensors, solar cells, biosensors and UV light emitters. The functional properties and photocatalytic behavior of ZnO is affected by the size and morphology, lattice defects and impurities presence, the type and amount of dopant. Currently, semiconductor photocatalysts are widely investigated due to their better properties compared to bulk scale photocatalysts and their potential applications [60].

Ag has been widely investigated for loading on the surfaces of various semiconductors due to its ability to separate the electron hole pairs by attracting the conduction band electrons and it is cheaper compared to other noble metals. The prepared Ag-ZnO photocatalysts can be evaluated by photo degradation of methylene blue (MB) as a pollutant model and exhibit higher efficiencies than the undoped ZnO NPs [61]. The degradation of methylene blue reacting with Photocatalytic oxidation can be shown as the following diagram [ 62].



Scheme 4: The Degradation Pathways of MB Reacting with Photocatalytic Oxidation.

As per the reviewed literatures, the degradation efficiency or the removal efficiency of the dye under investigation can be calculated using the following relation [23, 24].

$$\text{Degradation (\%)} = \frac{A_0 - A}{A_0} \times 100\%$$

Where  $A_0$  is absorbance of dye at initial stage,  $A$  is the final absorbance at time “ $t$ ” at  $\lambda_{\text{max}}$  of each dye.

### 3. Materials and Methods

#### 3.1. Experimental Site and Period

The study was carried out from July, 2020 to February, 2021; at Chemistry laboratory, Jimma University main campus, which is 346 Km south west of Addis Ababa, Ethiopia.

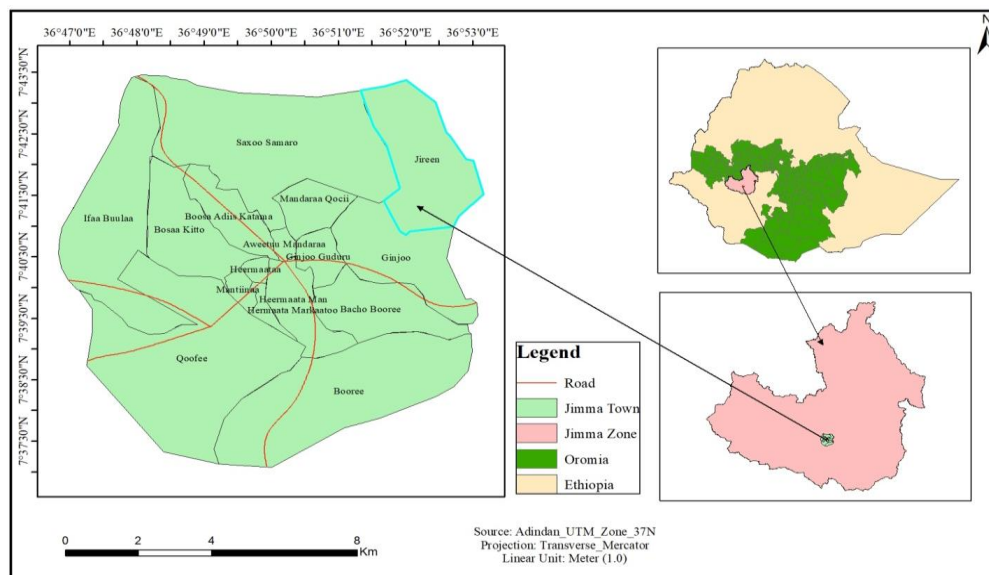


Figure 5: Map of the Study Area.

#### 3.2. Materials and Chemicals

All the chemicals and reagents used in this study were of analytical grade. Silver nitrate (99.5%, Alpha Chemika, India), Sodium hydroxide (99% NaOH, Sigma-Aldrich, UK), Zinc acetate dihydrate (98%  $C_4H_6O_4Zn \cdot 2H_2O$ , Merk, Germany), Ethanol (98%  $\pm$  1%, Ranchem Industry, Turkey), Methylene blue (Merk, Dermstadt, Germany), Iron (III) chloride hexahydrated (99%  $FeCl_3 \cdot 6H_2O$ , Faridabad-121005, India), Hydrochloric acid (38% HCl, Merk, Germany), Sulphuric acid (99%  $H_2SO_4$ , VWR International, France), Potassium iodide (99.5% KI, Alpha Chemika, India), Iodine (99.9%  $I_2$ , Faridabad-121005, India), Sodium chloride (99.9% NaCl, Loughborough, LE11 5RG, UK), Distilled water, Filter paper (Whatman No.1 and No.4), *Psidium Guajava* leaves.

#### 3.3. Apparatus

Water bath (Grant GLS400, England), Oven (Model: 158005/12, Gallenkamp, England), Thermometer, Mortar and Pestle, Digital balance (Adam, AFP-110L, UK), Magnetic stirrer plate

(Staffordshire, ST15, OSA; UK), Refrigerator (BEKO RRN 2650, Turkey), Centrifuge (Table Top Centrifuge, PLC-02; Taiwan), Centrifuge tubes, Beakers (150, 100, 250, 600 mL), Test tubes, Droppers, Graduated cylinders (10, 50, 100, 250 mL), Rack, Glass rode, Cuvettes, Erlenmeyer flasks (100, 250, 500 mL), Electrical grinder, Reagent bottles (125, 250, 500, 1000 mL), Volumetric flasks (100, 500, 1000 mL).

### **3.4. Scientific Instruments**

Double beam UV–Vis spectrophotometer (UV–Vis: SPECORD 200 PLUS-223, Germany), Single beam UV-Vis spectrophotometer (JENWAY-6705, Stone, staffs, ST15, OSA; UK), pH/Conductivity meter (Bante902P, China), X-ray diffractometer (XRD-7000, Drawell, Artist of Science, Shimadzu, USA), Fourier transform infrared spectrometry (FT-IR: PerkinElmer, Spectrum Two LITA, L1600300, UK).

### **3.5. Sample Collection and Preparation**

*Psidium guajava* (Guava) leaf was collected from the hills of Aba Jifar, around Jimma town, Oromia region, Ethiopia. The collected leaf was washed with tap water followed by distilled water to remove any dust particles, shade dried; ground to fine powder and stored at room temperature for further use. The aqueous leaf extract was prepared by taking 10 g of the Guava powder and dispersed into 120 mL of distilled water in a 500 mL Erlenmeyer flask. Then it was shaken for 24 h at room temperature and filtered with Whatman No 4 and No 1 filter paper. After extraction, the obtained reddish-brown filtrate was centrifuged at 4000 rpm for about 10 min to remove heavy insoluble biomaterials, the supernatant was collected and kept in refrigerator for further use [11, 12].

### **3.6. Preliminary Phytochemical Screening of the Plant Extract**

The preliminary phytochemical test was worked using standard procedures to identify varous classes of compounds [20, 43, 44]. Accordingly, the presence of alkaloids, flavonoids, phenols, tannins and saponins in the plant extract was examined.

#### **3.6.1. Test for phenols**

Ferric Chloride Test: Into the plant extract solution (4 mL) in a test tube, 2 drops of 0.1% ferric chloride ( $\text{FeCl}_3$ ) was added, shaken and dark green solution was observed [20, 43, 44, 63].

### **3.6.2. Test for Alkaloids**

Wagner's Test: The plant extract solution (4 mL) was taken into a test tube, 5 drops of Wagner's reagent (1 g of iodine and 3 g of potassium iodide were dissolved in 50 mL distilled water) was added into it. After shaken well, a reddish-brown precipitate result was formed [20, 43, 44, 63].

### **3.6.3. Test for Saponins**

Froth (foam) Test: Plant extract (2 mL) was placed in a test tube containing 4 mL of distilled water, shaken well for 20 seconds and the mixture was allowed to stand for 10 min. Then, a stable foam about 1 cm height was formed on the top layer of the mixture solution [20, 43, 44, 63].

### **3.6.4. Test for Flavonoids**

Alkaline Reagent Test: 4 mL of plant extract solution was treated with six drops of sodium hydroxide solution (1 M). The observed intense yellow color was disappeared on the addition of 4 drops of diluted hydrochloric acid (1 M) [20, 43, 44, 63].

### **3.6.5. Test for Tannins**

To 3 mL of plant extract, 2 mL of distilled water and 3 drops of 0.1%  $\text{FeCl}_3$  solution was added. After vigorously shaken, a blue-black color was observed [20, 43, 44, 63].

## **3.7. Optimization of Some Parameters**

As per the standards of previous reports, various parameters that regulate the experimental condition as being suitable for nanoparticle synthesis were optimized by varying one parameter and keep the other constant at a time to obtain the optimum values. Accordingly, effects of dopant concentration, volume of plant extract, pH and temperature were optimized before synthesizing of nanoparticles [64, 65].

## **3.8. Synthesis of ZnO Nanoparticles Using *Guava* Leaf Extract**

Zinc oxide NPs was synthesized according to the procedure reported in a literature [38]. 5 mL of aqueous leaf extract was added to 100 mL of 0.05 M of aqueous zinc acetate solution. The pH of the mixture was adjusted to 11 by adding 1 mL of 2 M NaOH in dropwise and stirred at room temperature for 20 min to achieve a pale-yellow solution. The suspended particles were purified

by dispersing in distilled water and centrifuged thrice. The found pale-white particles was washed with ethanol to remove the impurities from the final product. Then, a white powder was collected after drying at room temperature for one day and finally it was characterized.

### **3.9. Synthesis of Ag-ZnO NCs Using *Guava* Leaf Extract**

Solution of zinc acetate dihydrate (5 g) in 50 mL of distilled water was prepared at room temperature. 2 mL of an aqueous Silver nitrate solution ( $\text{AgNO}_3$ , 0.015M) was added into  $\text{C}_4\text{H}_6\text{O}_4\text{Zn}\cdot 2\text{H}_2\text{O}$  solution followed by 7 mL of *Guava* leaf extract in dropwise manner. The mixture was constantly stirred with magnetic stirrer at room temperature. After 30 minutes stirring, the mixture was centrifuged, washed three times with 5 mL of distilled water followed by mixture of ethanol and distilled water (1:1). The white precipitate was collected, dried at room temperature, used for characterization and application [4, 11, 12].

### **3.10. Characterizations of the Synthesized Ag-ZnO NCs**

The optical properties, coordinated functional groups and size of the green synthesized nanocatalysts were characterized by using UV-Vis, FT-IR and XRD techniques [12, 21, 66].

### **3.11. Photocatalytic Activity**

#### **3.11.1. Optimum Experimental Conditions**

Optimization is critical to maximize the rate of MB dye degradation. Some parameters having a crucial impact on the dye degrading capacity of the synthesized nanoparticles were optimized. The optimization was done for the effects of initial dye concentration, catalysts dose, pH, temperature and irradiation time [67-69].

#### **3.11.2. Photocatalytic Degradation of Methylene Blue Dye**

The photocatalytic activity of the synthesized Ag-ZnO NCs was evaluated by the degradation of methylene blue (MB) aqueous solution. 20 mg of photocatalyst was added into a 250 mL beaker containing MB solution (100 mL, 10 ppm). The mixture was stirred for 30 min at room temperature in the dark place to attain the adsorption-desorption equilibrium between the catalyst and MB. 5 mL of the mixture was received, centrifuged for 10 min and its absorbance was measured in the range of 400-800 nm before illumination. The solution was then exposed to

sunlight irradiation under stirring. At 20 min interval, 5 mL of the solution was sampled, centrifuged for 10 min, its absorbance was measured at maximum wavelength and the percentage degradation was determined until complete decolorization. Similarly, the bare MB dye solution was catalyzed under solar light irradiation and its degradation efficiency was compared with the reported results for Ag-ZnO NCs [12, 21, 23, 61, 70].

### **3.11.3. Recyclability of the Photocatalyst**

The re-usability of Ag-ZnO NCs catalyst was performed using dye decomposition method under natural sunlight [12]. 20 mg of Ag-ZnO NCs was added into a 250 mL beaker containing 100 mL of MB solution (10 ppm). The mixture was stirred for 30 min at room temperature in the dark place to attain the adsorption-desorption equilibrium between the catalyst and MB. 5 mL of the mixture was received, centrifuged for 10 min and its absorbance was measured in the range of 400-800 nm before illumination. The solution was then exposed to sunlight irradiation under stirring. At 20 min interval, 5 mL of the solution was sampled, centrifuged and its absorbance was measured at maximum wavelength constantly. After fully decolorization, the photocatalyst was centrifuged, washed by distilled water repeatedly and dried at room temperature before applying for next time. Using the same procedure, the photocatalytic degradation valuations were carried out for three cycles under sunlight and the percentage degradation was calculated for each trial and its degradation efficiency was related with the one that was catalyzed by Ag-ZnO nanocomposites [12, 21, 23, 61, 70].

## 4. Results and Discussion

### 4.1. Preliminary Phytochemical Screening of the *Guava* Leaf Extract

The reddish-brown aqueous extract was obtained from *Psidium guajava* leaves. Subsequently, the phytochemical constituents of the leaf extracts were analyzed and the results were indicated in Table 1 below [20, 43, 44, 63].

Table 1: Phytochemical Screening of *P. guajava* Leaf Extract.

S/No.	Secondary metabolites	Tests	Observations	Results
1	Phenols	Ferric chloride test	Dark green solution	+
2	Alkaloids	Wagner's test	Reddish brown precipitate	+
3	Saponins	Frothing (foam) test	A stable froth that persists for at least 2 min	+
4	Flavonoids	Alkaline reagent test	Yellow coloration which disappears on the addition of dilute HCl	+
5	Tannins	Ferric chloride	Blue-black coloration	+

+ = indicates the presence of phytoconstituents in *Psidium guajava* leaf extract

The phytochemical analysis of the water extract of the selected plant revealed the presence of phytoconstituents desired to be identified. As indicated in table 1, the *P. guajava* leaf extract was rich in phytochemical constituents of Phenols, Saponins, Flavonoids, Tannins and Alkaloids. Recently it was reported that these bioactive compounds contain the OH<sup>-</sup>, C=O-C, C=C and C=O functional groups and they are acting as reducing, capping and stabilizing agents in the synthesis of nanoparticles [12].





Figure 6: Phytochemical Analysis of *P. Guajava* Leaf Extract.

The phytochemical test results were similar with the earlier presented reports of the extract of the selected plant. Therefore, this study was confirmed the presence of important phytochemical constituents in the water extracts of *P. guajava* leaves [63, 71]. The phytochemical test of *guava* leaf extract showed the results that has good consistency with the reported value [63, 72].

#### 4.2. Optimization of Important Parameters

As the earlier reports indicated, investigating of physical parameters during the green biosynthesis of NPs is very important to manage its stability. The absorption peak was kept between 300 to 800 nm wavelength for each parameter [64, 65]. When a single parameter was optimized, other parameters were kept constant in each experiment.

In the study of the effect of pH, the sharp and short peaks were found at pH 8 and 9 with characteristic absorption peak of Ag-ZnO NCs at 378.8 nm. Mixture of the solution without adding of any acid or base was persisted at pH 8 whereas pH 9 was obtained after addition of few drops of 0.1 M NaOH. Therefore, pH 8 was favored as the optimum value than pH 9 as it was safest from alkaline solution. At lower pH 6 and higher pH 10, the absorption peaks were observed as broad peaks with long wavelength (380.7 nm) (Appendix A, A<sub>2</sub>) [64, 65]. Dopant concentration also affected the synthesis of Ag-ZnO NCs. Silver nitrate (AgNO<sub>3</sub>: 0.13%, 0.25%, 0.5% and 1%) was used as a dopant source [4]. A sharpest peak and shortest wavelength was

obtained for dopant (0.25%) corresponded to the small sized nanocomposites and it was endorsed as optimal value (Appendix B, B<sub>2</sub>).

Similarly, various volumes (3, 5, 7, 9 and 11 mL) of the extract was explored for optimization. A good peak with short wavelength value (376.9 nm) was recorded as an optimum volume for 7 mL of the plant extract (Appendix C, C<sub>3</sub>). The other factor known to be a major effector in the synthesis of nanoparticle is temperature. The optimal temperature for the synthesis of Ag-ZnO NCs was recorded as at room temperature (Appendix D, D<sub>1</sub>) [64].

After optimization of every parameter, green methods were employed for synthesis of both ZnO and Ag-ZnO nanoparticles. Moreover, the synthesized nanoparticles were centrifuged, washed and then a white colored powder was collected as the final product. The acquired results in good agreement with related literatures [4, 38].

### **4.3. UV-Vis Absorption Spectral Analysis**

Standard solution (8 ppm) was prepared for each sample. The extract, the synthesized ZnO and Ag-ZnO exhibited a UV-Vis absorption band at 309, 374 and 375 nm, respectively (fig. 7). The result is in good agreement with the previously reported values for ZnO NPs and Ag-ZnO NCs [73, 74]. Silver loading on ZnO is observed to shift the absorption edge to a longer wavelength that allows the Ag-ZnO catalysts to be active in the visible region. The surface plasmon band of Ag-ZnO NCs was red-shifted by 1 nm may be resulted due to the diffusion of the metallic silver into the crystal lattice of the semiconductor structure that the silver to be dispersed or inserted between the conduction and valence bands of the host material. The UV-Vis absorption peak difference between ZnO and Ag-ZnO NPs are might be due to the difference in their size and shape, which resulted from using similar precursors and working situation [75]. The shift increases with the increasing of the Ag amount in ZnO because more Ag inserted into the gap so that the gap becomes narrower than that of pure ZnO, shifting in the absorption wavelength to be increased [51, 52].

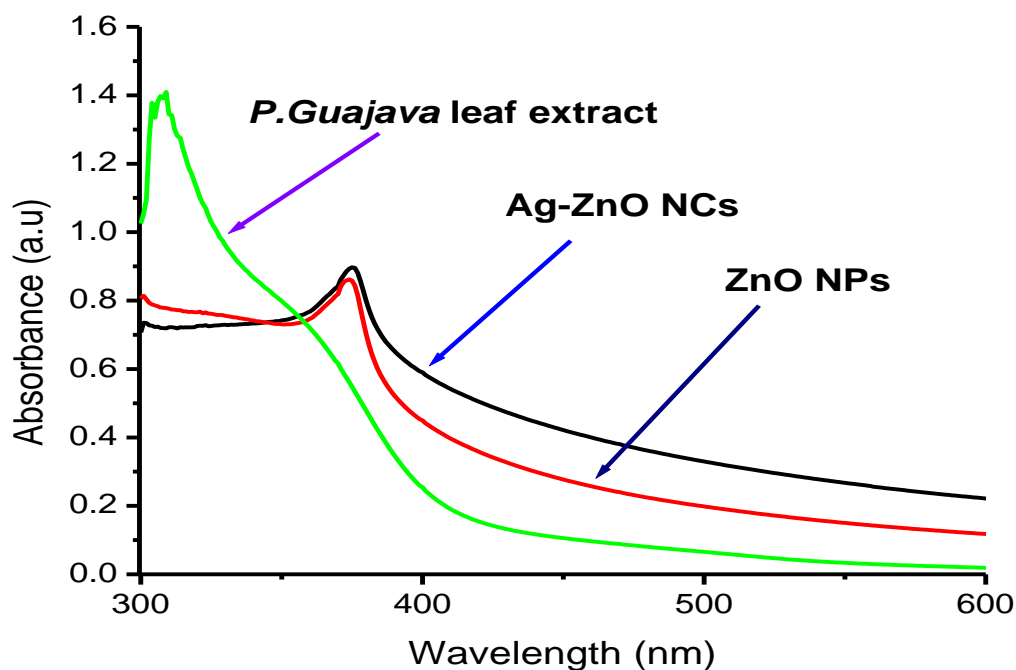


Figure 7: UV-Vis Absorption Spectra of A-ZnO NCs and ZnO NPs.

The presence of Ag NPs improved the band gap absorption in comparison to the bare ZnO NPs. The direct energy band gap was calculated using Tauc equation [4, 11].

$$\alpha h\nu = A(h\nu - E_g)^{1/2}$$

Where  $\alpha$  is absorption coefficient;  $h$  is Plank's constant;  $\nu$  is vibration frequency;  $A$  is constant and  $E_g$  is band gap. Tauc plot was obtained after extrapolation of UV-Vis data, plotting  $h\nu$  (energy) on X-axis and  $(\alpha h\nu)^2$  on Y-axis [4, 11]. According to Tauc plot, the band gap energy of ZnO and Ag-ZnO nanocatalysts were determined based on its adsorption edge wavelength and observed at 3.02 and 2.86 eV, respectively (fig. 8). The shift of absorption edge of nanocatalyst to a longer wavelength with Ag loading was resulted in smaller band gap energy [12, 52]. Having of this smaller band gap of the Ag-ZnO nanocomposite has a *vital* implication for various industrial applications and photocatalytic activity [12, 53].

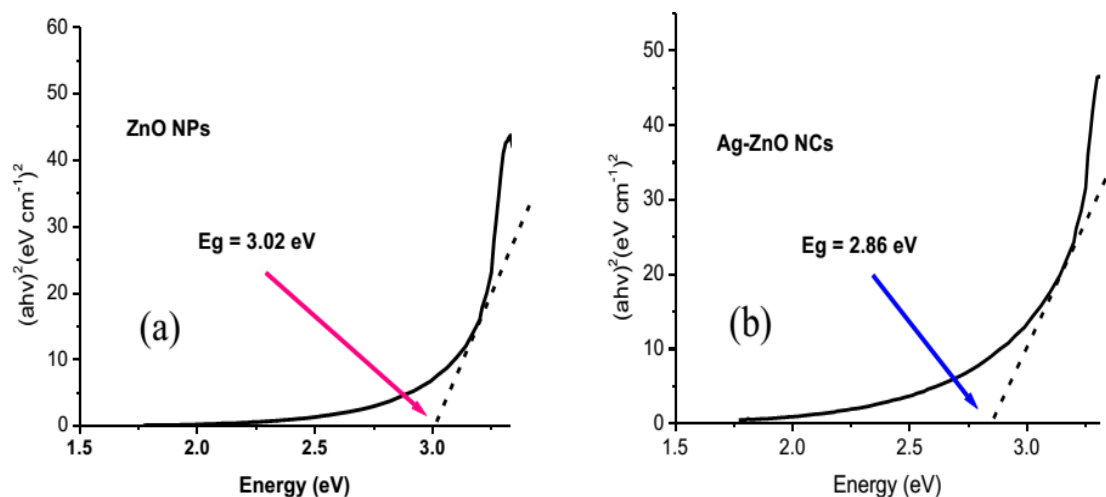


Figure 8: Tauc plot of ZnO NPs (a) and Ag-ZnO NCs (b) for direct band gap calculation.

#### 4.4. FT-IR Spectroscopic Study

The surface functional groups of a synthesized Ag-ZnO nanocomposite material were analyzed by FT-IR over a spectral range of 4000–400  $\text{cm}^{-1}$  at room temperature [56].

FT-IR analysis was performed to identify the functional groups responsible for reducing and stabilizing agents. As the former report showed, the phenolic groups of molecules are responsible for the reduction process and the stability of NPs due to the free amino and carboxylic groups [38].

A strong and broad absorption band, most probably in the range of 3600–3100  $\text{cm}^{-1}$  is corresponding to the hydroxyl groups (O-H) stretching (fig. 9a); it indicated the presence of alcoholic, or phenolic groups in the leaf extract with a wide variety of hydrogen bonding [76]. It could not be identified the exact position of the hydroxyl groups in the absorbance of the extract due to broadness of the peak. Then again, the narrow peaks was observed in both the synthesized ZnO NPs and Ag-ZnO NCs absorbance peaks which indicated the formation of nanoparticles. The peak intensity observed at  $\sim 3432 \text{ cm}^{-1}$  (fig. 9b) was indicated the coordination of O-H groups with the ZnO NPs. After the formation of Ag NPs on the surface of ZnO NPs, the intensity of ZnO peak was showed at  $\sim 3440 \text{ cm}^{-1}$  (fig. 9c) corresponded the stretching mode of the hydroxyl groups (O-H) which showed the binding of functional groups with Ag-ZnO NCs. There were a sharp and small peaks at 2979  $\text{cm}^{-1}$  and 2902  $\text{cm}^{-1}$  related with -C-H stretching vibrations of  $-\text{CH}_2$  and  $-\text{CH}$  groups, indicating the presence of aliphatic carbon (fig. 9a). The

strong and sharp peak at  $1644\text{ cm}^{-1}$  is assigned the presence of carbonyl ( $\text{-C=O}$ ) groups responsible for capping and stabilizing agents (fig. 9a). The  $\text{-C=O}$  stretching was and shifted to  $1629\text{ cm}^{-1}$  (fig. 9b),  $1634.5\text{ cm}^{-1}$  (fig. 9c) and became shorter ascribed that the carbonyl groups were capped the synthesized nanoparticles. The short peaks observed at  $1460\text{ cm}^{-1}$  and  $1384\text{ cm}^{-1}$  were indicated the presence of  $\text{-C=C}$  functional group and  $\text{N-O}$  in the extracts, respectively. There was also spectral band at  $1382\text{ cm}^{-1}$  which corresponded to the symmetric stretching of acetate species in the ZnO NPs. The absorption peak at  $1086\text{ cm}^{-1}$  is due to  $\text{C-N}$  stretching in primary amine or it might be the  $\text{C-O}$  stretching vibration of phenolic groups (fig. 9c). A short peak was appeared at  $879\text{ cm}^{-1}$  (fig. 9a) showed the existance of compounds such as polyphenols, carboxylic acid, polysaccharide, amino acid and proteins in the leaf extract. Then, its absorbance peak was reduced to  $873\text{ cm}^{-1}$  confirming that the synthesized Ag-ZnO NCs was good coordinated with such metabolites (fig. 9c). A small peak appeared at  $488\text{ cm}^{-1}$  is the characteristic absorption of  $\text{Zn-O}$  bond (fig. 9b). The FT-IR spectrum revealed the presence of active compounds in the extract which may substantially for nanoparticles stabilization as reported earlier [64, 76-79].

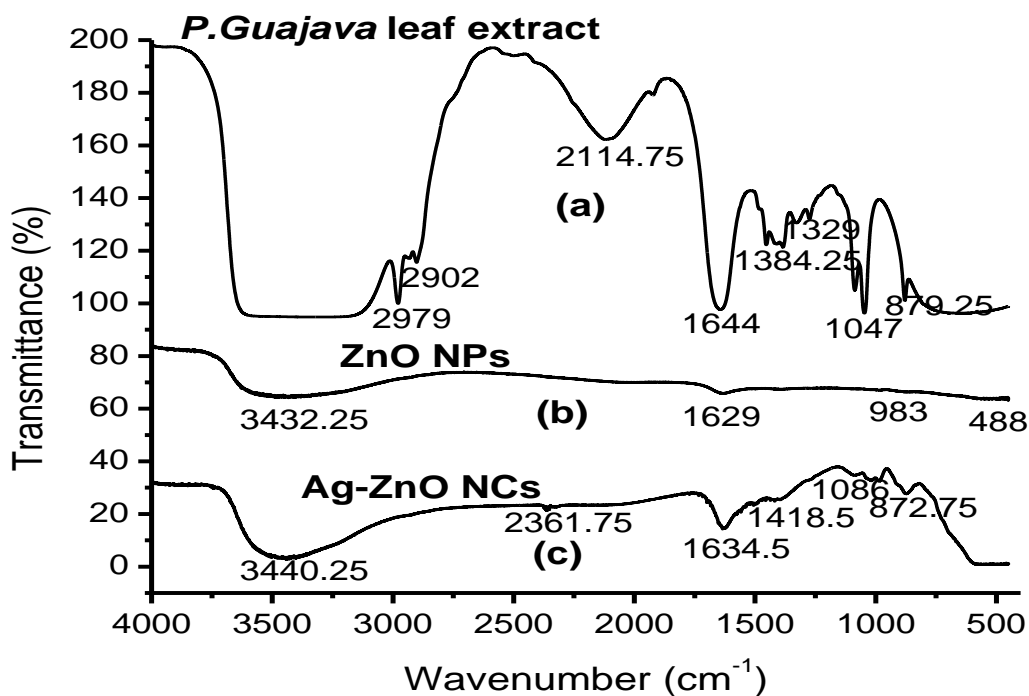


Figure 9: FT-IR Spectra of the Extract (a), ZnO NPs (b) and Ag-ZnO NCs (c).

#### 4.5. XRD Analysis

The crystal structure and diffraction patterns of ZnO NPs and Ag-ZnO NCs were recognized by X-ray diffraction (XRD) in  $2\theta$  range of  $25^\circ$ - $80^\circ$  with scan rate  $5^\circ/\text{min}$  [80]. The patterns indicated with distinct peaks at  $2\theta$ :  $31.69^\circ$ ,  $34.52^\circ$ ,  $36.44^\circ$ ,  $47.68^\circ$ ,  $56.72^\circ$  and  $68.04^\circ$  which correspond to the crystal planes of the undoped ZnO NPs indexed to the (100), (002), (101), (102), (110) and (112) reflection planes, respectively (fig. 10a). These diffraction peaks are related to the well crystalline hexagonal wurtzite structure of ZnO NPs as indicated by the Joint Committee on Powder Diffraction Standards (JCPDS No: 36-1451) [81, 82]. The additional peaks observed in the XRD pattern of ZnO may be contributed from the precursor zinc acetate dihydrate [83, 84]. After doping of ZnO by Ag, there were a change in intensity peaks and slightly shift of diffraction angles observed. Specifically, the weak peaks looked at  $37.67^\circ$ ,  $42.89^\circ$ ,  $61.81^\circ$  and  $72.83^\circ$  were related to the intense (111), (200), (220) and (311) reflection (fig. 10b). However, the intense peak at  $37.67^\circ$  was not observed well, it may be resulted from low in amount of the dopant. It was in good agreement with the already reported value and with standard data card (JCPDS No: 04-0783), corresponded to face-centered cubic (fcc) metallic structure of Ag [80, 81]. Appearance of those peaks in the diffraction pattern referred to the presence of metallic Ag content on the ZnO surface. The intensity of Ag peak was small because the Ag core was completely covered by the ZnO shell, indicated the formation of Ag-ZnO NCs [80-82].

From the XRD analysis, the diffraction peaks were the narrow and low-intensity peak of (100) and (002) as compared with ZnO NPs in (fig. 10) because of the effect of Ag ions as a dopant in ZnO structures. From these results, most of the silver ions are located on the surfaces or the interface of the ZnO structure, and there are some of silver ion peaks not detected in XRD analysis because of the low content of metallic Ag and less dispersion. The average crystallite size calculated using Debye-Scherrer's equation [12, 45, 51, 54, 55] were found to be 22, 26 nm for ZnO NPs and Ag-ZnO NCs products, respectively. These results have good agreement with the previous studies [80, 81].

$$D = \frac{0.89\lambda}{\beta \cos\theta}$$

Where,  $D$  = average crystallite size,  $\lambda$  is wavelength of X-ray beam ( $1.54056\text{\AA}$ ),  $\theta$  is the Bragg diffraction angle in degree,  $\beta$  is full width at half maxima (FWHM) of XRD peak.

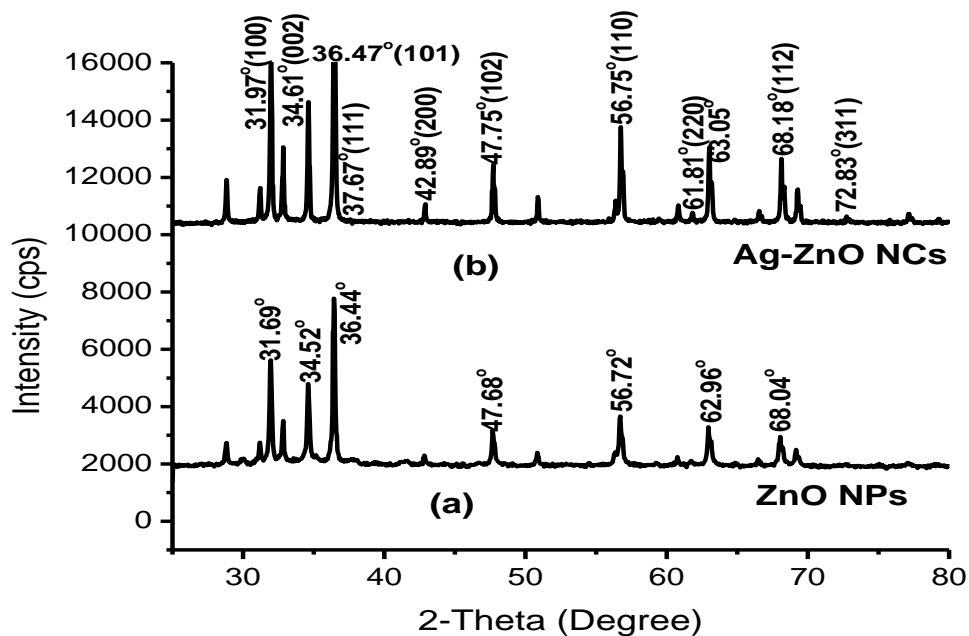


Figure 10: XRD Pattern of Ag-ZnO NCs (a) and ZnO NPs (b).

#### 4.6. Optimization of Photocatalytic Parameters

For each parameter, the decolorization and percentage dye degradation efficiency (removal efficiency) was calculated using the following formula [23, 32]:

$$R = \frac{C_0 - C}{C_0} \times 100\% = \frac{A_0 - A}{A_0} \times 100\%$$

Where  $C_0$ ,  $C$ ,  $A_0$  and  $A$  are concentration and absorbance of dye at reaction condition time (0) and (t) min respectively.

##### 4.6.1. Effect of Ag-ZnO NCs Catalyst Dose

The prepared Ag-ZnO NCs was used to evaluate the degradation of methylene blue (MB). In order to find out the optimum concentration, the effect of various amounts of photocatalyst (10, 15, 20 and 25 mg) was studied at constant pH, concentration of dye, temperature and contact time. It was observed that increasing of the catalyst dose from 10 to 20 mg enhanced the degradation rate. It indicates that the dose of Ag-ZnO up to 20 mg produce higher amounts of species having active sites (hydroxyl and superoxide radicals) on the photocatalyst surface and

provided the best photocatalytic degradation efficiency. However, the degradation performance decreases at further increase in the catalyst dose [67, 68]. This could be due to increase in turbidity of the working system that scatters solar radiation, delimits the photoexcitation efficiency to activate the catalyst surface and the photocatalytic activity decreases [67, 69]. The obtained results showed that an optimum amount of catalyst for decolorization of the dye mixture was 20 mg as greater than 98% of dye degradation was achieved at 100 min [69].

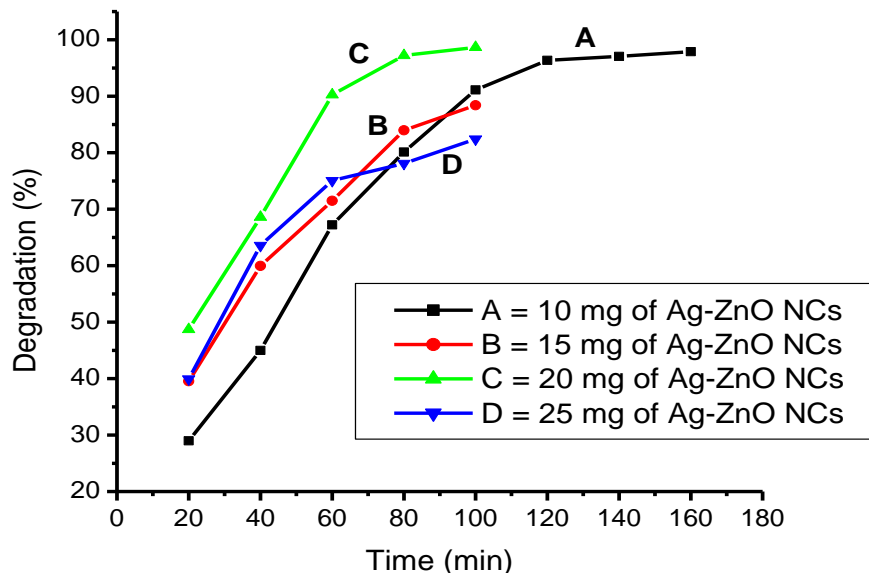


Figure 11: Effects of Ag-ZnO Dose on MB Photodegradation.

#### 4.6.2. Effect of Initial Dye Concentration

To determine the optimal amount of dye, other parameters like pH, temperature, catalyst dose and irradiation time were kept constant and various concentrations (6, 8, 10, 12 ppm) of MB dye were used separately.

The degradation efficiency of dye was decreased by increasing concentration of the dye to more than 10 ppm. This incidence is due to the fact that more dye molecules adsorb on the surface of the catalyst and hinders the photons reach into the surface of the Ag-ZnO so that the active sites for the generation of hydroxyl radicals can be reduced [68, 69]. More than 98% of MB (10 ppm) dye was degraded at 100 min so that it was determined as initial optimal concentration ( fig. 12).



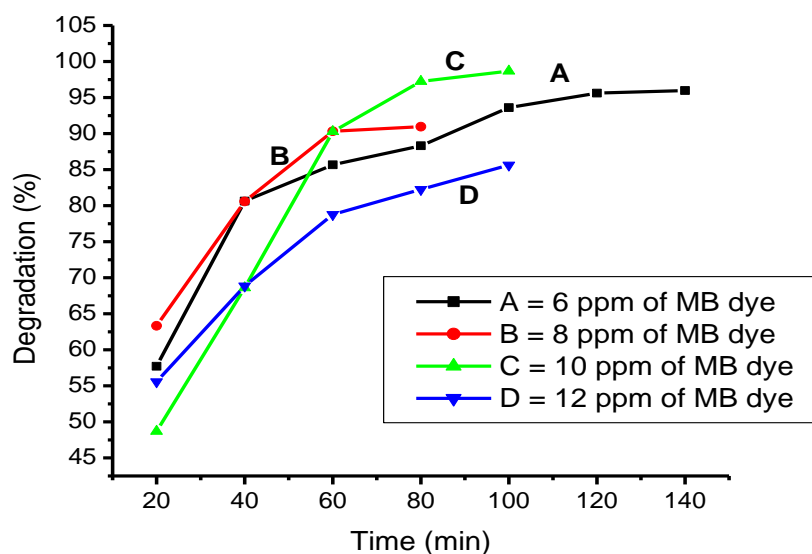


Figure 12: Effects of MB Dye Concentration on Photodegradation.

#### 4.6.3. Effect of pH and Point of Zero Charge

One of a very important parameters affecting the photodegradability of dye pollutants is the pH of the working solution [67, 69]. Point of zero charge (PZC) was determined before optimization for pH effects carried out. PZC is the pH at which the net charge of particle surface is equal to zero or neutral. 40 mL of 0.1 M NaCl was poured into six vials separately; the pH was adjusted by 0.1 M HCl and 0.1 M NaOH in the range of 2, 4, 6, 8, 10, 12 and is denoted as  $pH_i$  for each. Then, 20 mg of Ag-ZnO NCs was added, shaken for 24 h and after settling, the pH values of the supernatant in each vial was measured and denoted as  $pH_f$ . The PZC was obtained from the intersection point of the plot of  $\Delta pH$  ( $pH_f - pH_i$ ) versus  $pH_i$  (fig. 13). Below this value, the surface of the catalyst is positively charged and is always easier to adsorb an anion, whereas beyond this value, it is negatively charged particle surface so that it adsorbs a cation on a negatively charged surface [85; 86].

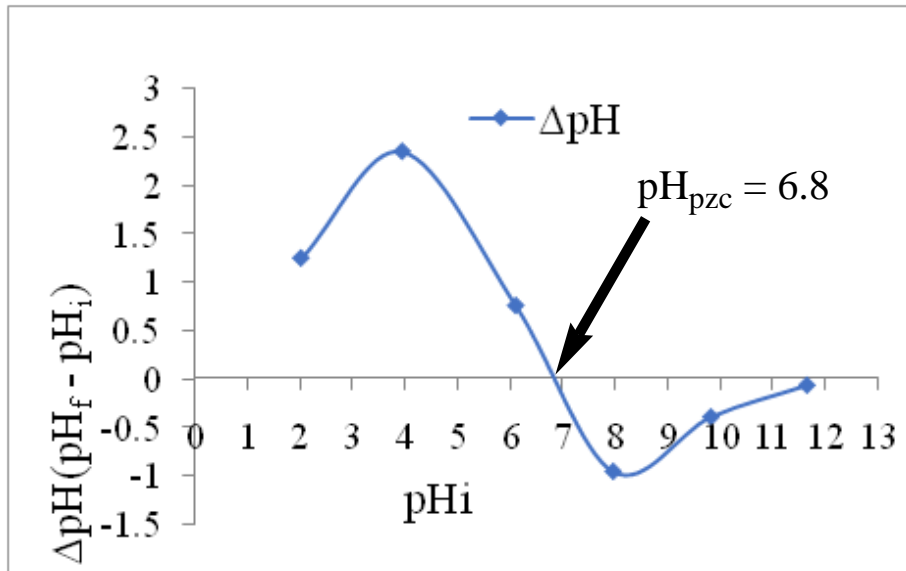


Figure 13: Determination of pH at Point of Zero Charge.

In the study, solutions of HCl (0.1 M) and NaOH (0.1 M) were used to control the pH of MB (10 ppm) solution mixture that containing 20 mg of nanocatalyst. It was adjusted within the range of pH (4, 6, 7.4, 9 and 11) before starting the photocatalytic degradation reaction. Then by following the photocatalytic procedure, the experiment for effects of pH on dye degradation was conducted and the obtained results showed the highest degradation efficiency of 98.67% at pH 7.4. Therefore, pH 7.4 was accepted as the optimized value of the working condition for photocatalytic degradation.

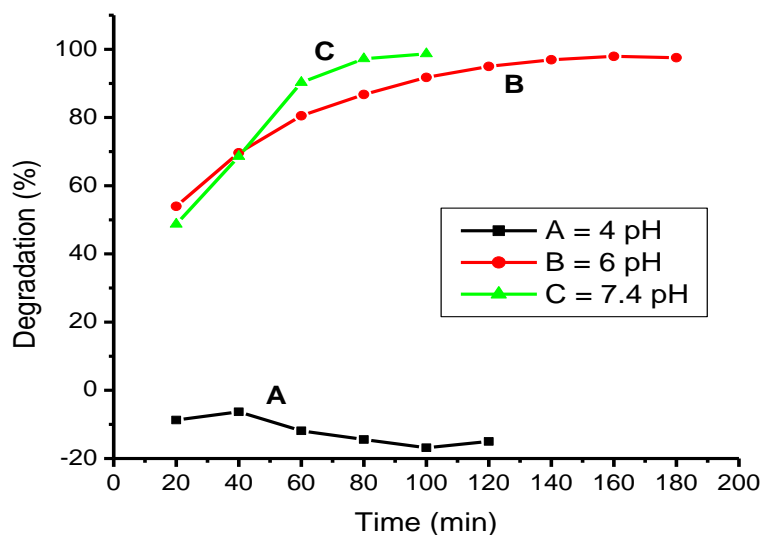


Figure 14: pH Effects on Percent Degradation of MB Dye.

As seen from fig. 14, the lowest photocatalytic degradation efficiency was noticed at pH 4. This small value is due to the repulsion occurred between the positively charged surface of the Ag-ZnO nanocatalyst and positive groups of MB molecules, which forces the photodegradation efficiency is being decreased [68, 69]. Meanwhile, demethylation and photodegradation of methylene blue were observed in the presence of the Ag-ZnO NCs at pHs 7.4 and above [68, 69]. At pH 9, about 82% of MB was degraded and completely decolorized at onset of 20 min. In case of pH 11, the mixture of the dye was decolorized as soon it exposed as sunlight. This condition was confirmed that at pH greater than optimal value, the surface of the catalyst can be negatively charged due to excess amount of hydroxyl ions (OH<sup>-</sup>) that have the ability to search holes on the Ag-ZnO surface where the excess OH<sup>-</sup> ions converted to hydroxyl radicals. Thus, it was increased the density of ·OH radicals and the coordinative contact with positive group of MB dye in which it facilitate the photodegradation performance as to be enhanced [67-69].

#### 4.6.4. Effect of Irradiation Time

The effect of irradiation time on the degradation efficiency of the photocatalyst was examined at time intervals ranged from 20 to 120 min for the catalyzed and from 20 to 200 min for the uncatalyzed MB both under UV light, using 20 mg of Ag-ZnO catalyst and 10 ppm of MB dye solution at pH 7.4 and at room temperature. The percent degradation was evaluated as follows [23, 24, 32].

$$\text{Degradation (\%)} = \frac{A_0 - A}{A_0} \times 100\%$$

At 60, 80 and 100 min, the percent degradation of the dye was 90.27%, 97.23% and 98.67%, respectively. After 100 min, the dye mixture was completely decolorized and photodegradation was accomplished so that the 100 min was taken as the optimal irradiation time.

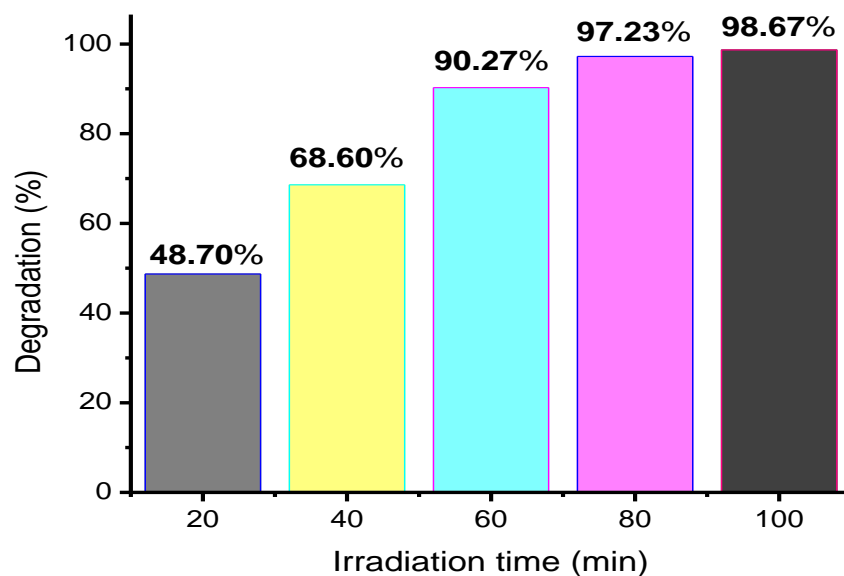
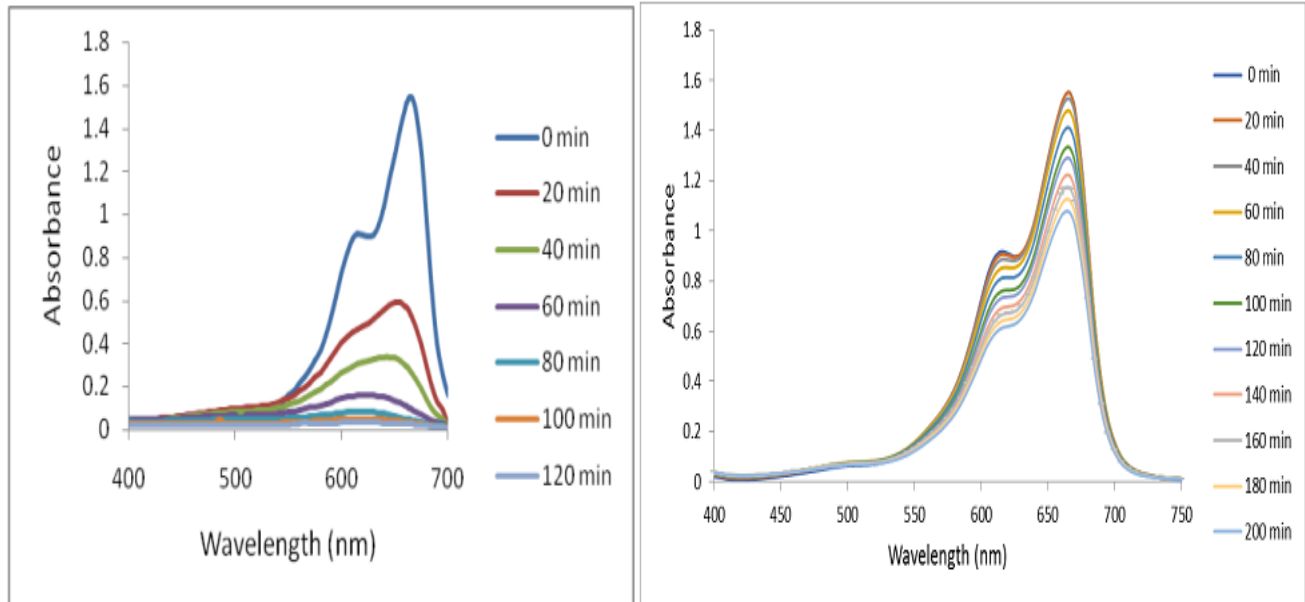


Figure 15: Effects of Irradiation Time on Photodegradation of MB.

In the former report, the highest photodegradation of MB (degraded about 96%) was achieved at 100 min by Ag doped ZnO nanocatalyst. In fact, the Ag-ZnO sample showed high efficiency from the evaluated optimal irradiation times [87].

#### 4.7. Photocatalytic Degradation Activity

Under optimized conditions, the photocatalytic efficiencies of the Ag-ZnO NPs was evaluated by degrading of MB. The MB molecules showed absorption peak at 665 nm [88]. The absorbance of MB at 665 nm was intensely diminished after 20 to 120 min of irradiation in the presence of Ag-ZnO catalyst and was able to motivate dye decoloration (Appendix E, E<sub>1</sub>). However, in the absence of Ag-ZnO photocatalyst, the absorbance of MB was slowly reduced even after 200 min irradiation and was unable to decolorize the dye (Appendix E, E<sub>2</sub>). These results were consistent with the previously conducted research [87].



(a)

(b)

Figure 16: UV-Vis of MB Catalyzed by Ag-ZnO NCs (a) and Uncatalyzed MB (b).

The percentage degradation for the catalyzed and uncatalyzed MB was calculated using the following formula [24] and summarized in table 2 below.

$$\text{Degradation (\%)} = \frac{A_0 - A}{A_0} \times 100\%$$

Where,  $A_0$  is the initial and  $A$  is the final absorbance at  $\lambda_{\text{max}}$  of dye at each time  $t$ .

Table 2: Percent Degradation of Both Catalyzed and Uncatalyzed MB.

Time (min)	$\lambda_{\max}$ (nm)	MB (Catalyzed)		MB (Uncatalyzed)	
		Absorbance	%D	Absorbance	%D
0	665	1.5459	---	1.5510	---
20	665	0.5385	65.17	1.5509	0.01
40	665	0.2719	82.41	1.5281	1.48
60	665	0.0977	93.68	1.4808	4.53
80	665	0.0469	96.97	1.4123	8.94
100	665	0.0346	97.76	1.3363	13.84
120	665	0.0270	98.25	1.2895	16.86
140	665	---	---	1.2229	21.15
160	665	---	---	1.1722	24.42
180	665	---	---	1.1283	27.25
200	665	---	---	1.0768	30.57

The results indicated that the degradation efficiency of Ag-ZnO photocatalyst was increased as the illumination time increased. The dye mixture catalyzed with Ag-ZnO NCs was fully decolorized and more than 98% was photocatalytically degraded after 120 min irradiation time; however, the dye catalyzed only under solar light was degraded about 31% even after 200 min irradiation. This evidence confirmed that the Ag-ZnO catalyst synthesized by plant leaf extract mediated has a good efficiency to remove the MB dye pollutant. The percent degradation of MB catalyzed and non-catalyzed by nanoparticles, respectively was illustrated below (fig. 17).

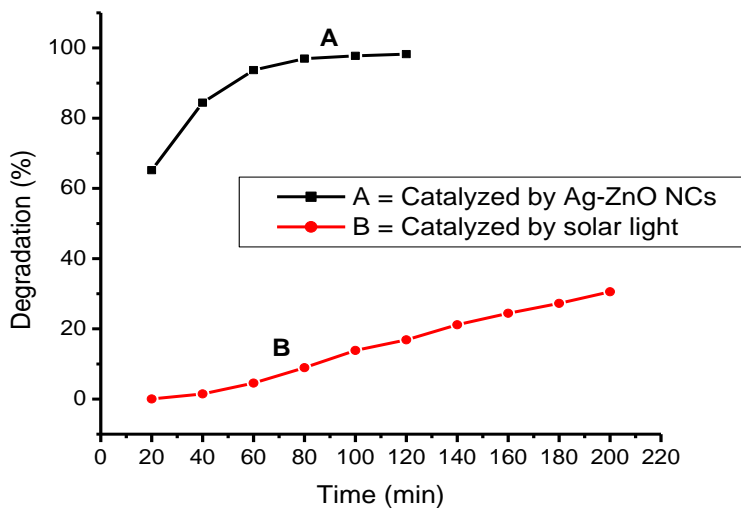


Figure 17: Photocatalytic Percent Degradation Efficiency of MB.

#### 4.8. Re-usability of the Photocatalyst

The re-usability of the photocatalyst was sequentially performed and the percent degradation was determined after 60 min sunlight irradiation for three cycles. The photodegradation outcomes depict 90.27%, 82.54% and 76.43% of dye degradation for 1<sup>st</sup>, 2<sup>nd</sup> and 3<sup>rd</sup> cycles, respectively. It was illustrated by fig. 18 below.

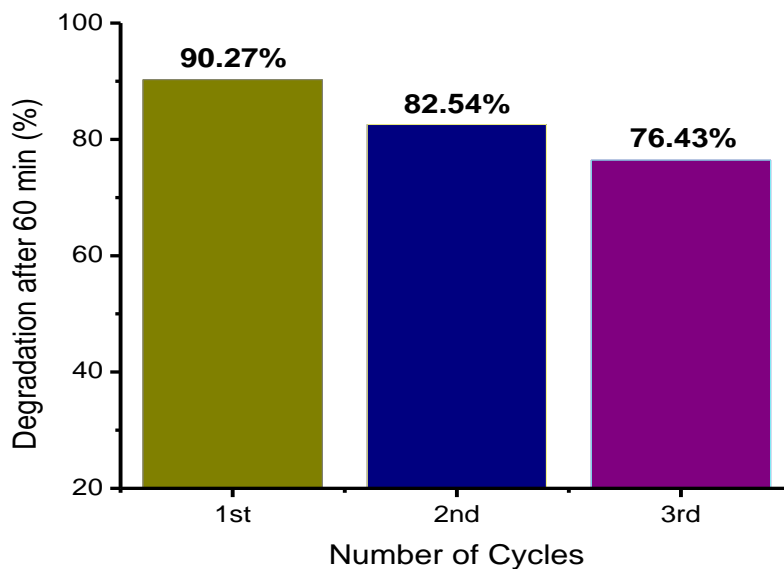


Figure 18: Cycling Times of the Photodegrading MB Applying ZnO-Ag NCs Catalyst.

The main advantage of heterogeneous nanocatalyst is its re-usability. The catalyst re-usability is an important performance of the photocatalytic process, because a significant cost reduction on the treatment of dye effluent is crucial. To assess the stability of the photocatalyst, Ag-ZnO NCs was used for photocatalytic runs. The results in fig. 18 indicated that the activity of Ag-ZnO slightly decreased and MB degradation was achieved after three runs from 1<sup>st</sup> cycle (90.27%) to 3<sup>rd</sup> cycle (76.43%) [89]. Also, the photocatalytic activity of the samples only minimally decreases, due to the unavoidable loss of photocatalysts during the cycle processes [90].



## 5. Conclusions and Recommendations

### 5.1. Conclusions

The present study established an eco-friendly method to synthesis ZnO NPs and Ag-ZnO NCs through a novel single step green method using *Psidium guajava* leaf extract. Silver nitrate and zinc acetate dihydrated as the precursor materials were used. The phytochemical screening results verified the presence of phenols, saponins, alkaloids and flavonoids in the leaf extracts. Characterizations were accomplished using UV-Vis, FT-IR and XRD techniques, confirming the successful formation of ZnO NPs and Ag-ZnO NCs. The UV-Vis absorbance peak was given a clue about the crystallite size of ZnO and Ag-ZnO NPs. The results showed that the doping of ZnO NPs by Ag was improved the band gap of the synthesized Ag-ZnO NCs. Presence of main functional groups was observed from FT-IR spectrum. The photocatalytic degradation of Ag-ZnO NCs was investigated using methylene blue dye in the presence of visible light and the results ensured a drastic improvement from the earlier reports of the photocatalytic activity of Ag-ZnO NCs. Hence, the designed plant leaf mediated Ag-ZnO NCs synthesis have provided avenues with the enhancement of high-efficiency of its photocatalytic degradation activity, so that the desired objectives were fruitfully attained.

### 5.2. Recommendations

From this study, the following recommendation has been forwarded:

- Additional characterization is significant for the surface morphology, distribution, composition, stability, moisture content, size and shape of the synthesized Ag-ZnO NCs using SEM, TEM, EDX and TGA techniques.
- It is better if further investigation is conducted upon the plant extracts mediated Ag-ZnO NCs in order to identify the efficiency of photocatalytic degradation activity.
- It is also recommended that the synthesized Ag-ZnO NCs needs additional study for more applications like sensor and antimicrobial activity.

## References

1. Bhakya, S.; Muthukrishnan, S.; Sukumaran, M.; Muthukumar, M.; Kumar, S. T.; Rao, M. V. Catalytic Degradation of Organic Dyes Using Synthesized Silver Nanoparticles: A Green Approach. *Journal of Bioremediation and Biodegradation*. **2015**, *6*, 1.
2. Mata, R.; Bhaskaran, A.; Sadras, S. R. Green-synthesized Gold Nanoparticles from *Plumeria Alba* Flower Extract to Augment Catalytic Degradation of Organic Dyes and Inhibit Bacterial Growth. *Particuology*. **2016**, *24*, 78-86.
3. Saoud, M. K.; Saleh, B. N.; Alsoubaihi, M. R. Synthesis and Characterization of Ag-ZnO Visible Light Photocatalyst. *Journal of Materials, Methods and Technologies*. **2013**, *7*, 415-423.
4. Ahmad, K. S.; Jaffri, S. B. Phytosynthetic Ag Doped ZnO Nanoparticles: Semiconducting Green Remediators. *Open Chemistry*. **2018**, *16*, 556–570.
5. Ghoranneviss, M.; Soni, A.; Talebitaher, A.; Aslan, N. Nanomaterial Synthesis, Characterization, and Application. *Journal of Nanomaterials*. **2015**, 1-2.
6. Malik, T.; Chauhan, G.; Murthy, R.S.R.; Goyal, A. K. “Fusion and Binding Inhibition” Key Target for HIV-1 Treatment and Pre-exposure Prophylaxis: Targets, Drug Delivery and Nanotechnology Approaches. *Drug Delivery*. **2017**, *24*, 608–621.
7. Abbasi, B. H.; Shah, M.; Hashmi, S. S.; Nazir, M.; Naz, S.; Ahmad, W.; Khan, I. U.; Hano, C. Green Bio-Assisted Synthesis, Characterization and Biological Evaluation of Biocompatible ZnO NPs Synthesized from Different Tissues of Milk Thistle (*Silybum marianum*). *Nanomaterials*. **2019**, *9*, 1171.
8. Tan, N. P. B.; Lee, C. H.; Li, P. Green Synthesis of Smart Metal/Polymer Nanocomposite Particles and Their Tuneable Catalytic Activities. *Polymers*. **2016**, *8*, 105.
9. Paulkumar, K.; Gnanajobitha, G.; Vanaja, M.; Pavunraj, M.; Annadurai, G. Green Synthesis of Silver Nanoparticle and Silver-based Chitosan Bio Nanocomposite Using Stem Extract of *Saccharum Officinarum* and Assessment of its Antibacterial Activity. *Advances in Natural Sciences: Nanoscience and Nanotechnology*. **2017**, *8*, 035019.

10. Venkatachalam, P.; Sangeetha, P.; Geetha, N.; Sahi, S. V. Phytofabrication of Bioactive Molecules Encapsulated Metallic Silver Nanoparticles from *Cucumis Sativus* L. and its Enhanced Wound Healing Potential in Rat Model. *Journal of Nanomaterials*. **2015**, *2015*, 1-9.
11. Jaffri, S. B.; Ahmad, S. K. Foliar-mediated Ag-ZnO Nanophotocatalysts: Green Synthesis, Characterization, Pollutants Degradation, and in Vitro Biocidal Activity. *Green Processing and Synthesis*. **2019**, *8*, 172–182.
12. Zare, M.; Namratha, K.; Alghamdi, S.; Mohammad, Y. H. E.; Hezam, A.; Zare, M.; Drmash, Q. A.; Byrappa, K.; Chandrashekar, B. N.; Ramakrishna, S.; Zhang, X. Novel Green Biomimetic Approach for Synthesis of Ag-ZnO Nanocomposite; Antimicrobial Activity Against Food-borne Pathogen, Biocompatibility and Solar Photocatalysis. *Scientific Reports* **2019**, *9*, 1-15.
13. Singh, T.; Jyoti, K.; Patnaik, A.; Singh, A.; Chauhan, R.; Chandel, S. S. Journal of Genetic Engineering and Biotechnology: Biosynthesis, Characterization and Antibacterial Activity of Silver Nanoparticles Using an Endophytic Fungal Supernatant of *Raphanus Sativus*. *Journal of Genetic Engineering and Biotechnology*. **2017**, *15*, 31-39.
14. Khurshid, Z.; Zafar, M.; Qasim, S.; Shahab, S.; Naseem, M.; AbuReqaiba, A. Advances in Nanotechnology for Restorative Dentistry. *Materials*. **2015**, *8*, 717–731.
15. Suwan, T.; Khongkhunthian, S.; Okonogi, S. Antifungal Activity of Polymeric Micelles of Silver Nanoparticles Prepared from *Psidium Guajava* Aqueous Extract. *Drug Discoveries and Therapeutics*. **2019**, *13*, 62-69.
16. Moteriya, P.; Padalia, H.; Chanda, S. Green Biosynthesis of Silver Nanoparticles Using *Psidium Guajava* L. leaf Extract and Antibacterial Activity Against Some Pathogenic Microorganisms. *Journal of Pharmaceutical Research*. **2014**, *8*, 1579-1585.
17. Bouchoukh, I.; Hazmoune, T.; Boudelaa, M.; Bensouici, C.; Zellagui, A. Anticholinesterase and Antioxidant Activities of Foliar Extract from a Tropical Species: *Psidium Guajava* L. (Myrtaceae) Grown in Algeria. *Current Issues in Pharmacy and Medical Sciences*. **2019**, *32*, 160-167.

18. Somchaidee, P.; Tedsree, K. Green Synthesis of High Dispersion and Narrow Size Distribution of Zero-valent Iron Nanoparticles Using *Guava* Leaf (*Psidium Guajava* L.) Extract. *Advances in Natural Sciences: Nanoscience and Nanotechnology*. **2018**, *9*, 035006.
19. Roberson, M.; Rangari, V.; Jeelani, S.; Samuel, T.; Yates, C. Synthesis and Characterization Silver, Zinc Oxide and Hybrid Silver/Zinc Oxide Nanoparticles for Antimicrobial Applications. *Nano Life*. **2014**, *4*, 1440003.
20. Sharma, V.; Agarwal, A.; Chaudhary, U.; Singh, M. Phytochemical Investigation of Various Extracts of Leaves and Stems of *Achyranthes Aspera* Linn. *International Journal of Pharmacy and Pharmaceutical Sciences*. **2013**, *5*, 317-320.
21. Mohammadzadeh, S.; Olya, M. E.; Arabi, A. M.; Shariati, A.; Nikou, M. R. K. Synthesis, Characterization and Application of Ag-ZnO as a Nanophotocatalyst for Organic Compounds Degradation, Mechanism and Economic Study. *Journal of Environmental Sciences*. **2015**, *35*, 194–207.
22. Khaldakar, M.; Butala, D. The Synthesis and Characterization of Metal Oxide Nanoparticles and its Application for Photocatalysis. *International Journal of Scientific and Research Publications*. **2017**, *7*, 499-504.
23. Saeed, M.; Muneer, M.; Khosa, M. K. K.; Akram, N.; Khalid, S.; Adeel, M.; Nisa, A.; Sherazi, S. *Azadirachta Indica* Leaves Extract Assisted Green Synthesis of Ag-TiO<sub>2</sub> for Degradation of Methylene Blue and Rhodamine B Dyes in Aqueous Medium. *Green Processing and Synthesis*. **2019**, *8*, 659-666.
24. Welderfael, T.; Yadav, O. P.; Taddesse, Abi M.; Kaushal, J. Synthesis, Characterization and Photocatalytic Activities of Ag-N-Codoped ZnO Nanoparticles for Degradation of Methyl Red. *Bulletin of the Chemical Society of Ethiopia*. **2013**, *27*, 221-232.
25. Bazant, P.; Sedlacek, T.; Kuritka, I.; Podlipny, D.; Holcapkova, P. Synthesis and Effect of Hierarchically Structured Ag-ZnO Hybrid on the Surface Antibacterial Activity of a Propylene-Based Elastomer Blends. *Materials*. **2018**, *11*, 363.

26. Upadhyaya, H.; Shome, S.; Sarma, R.; Tewari, S.; Bhattacharya, M. K.; Panda, S. K. Green Synthesis, Characterization and Antibacterial Activity of ZnO Nanoparticles. *American Journal of Plant Sciences*. **2018**, *9*, 1279-1291.
27. Singh, P.; Kim, Y. J.; Wang, C.; Mathiyalagan, R.; Yang, D. C. The Development of a Green Approach for the Biosynthesis of Silver and Gold Nanoparticles by Using *Panax Ginseng* Root Extract, and Their Biological Applications. *Artificial Cells, Nanomedicine, and Biotechnology*. **2016**, *44*, 1150–1157.
28. Parveen, K.; Banse, V.; Ledwani, L. Green Synthesis of Nanoparticles: Their Advantages and Disadvantages. In *AIP Conference Proceedings*. **2016**, *1724*, 020048.
29. Shriver and Atkins'; Inorganic Chemistry, 5<sup>th</sup> Ed., Oxford University Press, Great Britain, 2010, 1-824.
30. Srivastava, R. Synthesis and Characterization Techniques of Nanomaterials. *International Journal of Green Nanotechnology*. **2012**, *4*, 17-27.
31. Shriver and Atkins'; Inorganic Chemistry, 6<sup>th</sup> Ed., Oxford University Press, Great Britain, **2014**, 1-875.
32. Nguyen, L.T.T.; Nguyen, L. T. H.; Duong, A.T. T.; Nguyen, B. D.; Hai, N. Q.; Chu, V. H.; Nguyen, T. D.; Bach, L. G. Preparation, Characterization and Photocatalytic Activity of La-Doped Zinc Oxide Nanoparticles. *Materials*. **2019**, *12*, 1195.
33. Khan, Y.; Qasimnasar, M.; Numan, M.; Ullah, I.; Shinwari, K. Z. Biomimetic Synthesis of Silver Nanoparticles for Breast Cancer Therapeutics and its Mechanism. *International Journal of Nanotechnology and Nanomedicine*. **2018**, *3*, 1-9.
34. Joseph, S.; Mathew, B. Microwave-assisted Green Synthesis of Silver Nanoparticles and the Study on Catalytic Activity in the Degradation of Dyes. *Journal of Molecular Liquids*. **2015**, *204*, 184-191.
35. Gour, A.; Jain, N. K. Advances in Green Synthesis of Nanoparticles. *Artificial Cells, Nanomedicine, and Biotechnology*. **2019**, *47*, 844–851.

36. Galstyan, V.; Bhandari, M. P.; Sberveglieri, V.; Sberveglieri, G.; Comini, E. Metal Oxide Nanostructures in Food Applications: Quality Control and Packaging. *Chemosensors*. **2018**, *6*, 16.
37. Palem, R. R.; Ganesh, S. D.; Kronekova, Z.; Sláviková, M.; Saha, N.; Saha, P. Green Synthesis of Silver Nanoparticles and Biopolymer Nanocomposites: A Comparative Study on Physico-chemical, Antimicrobial and Anticancer Activity. *Bulletin of Materials Science*. **2018**, *41*, 55.
38. Venkatesan, A.; Prabakaran, R.; Sujatha, V. Phytoextract-mediated Synthesis of Zinc Oxide Nanoparticles Using Aqueous Leaves Extract of *Ipomoea Pes-caprae* (L).br Revealing its Biological Properties and Photocatalytic Activity. *Nanotechnology for Environmental Engineering*. **2017**, *2*, 8.
39. Azizi, S.; Mohamad, R.; Rahim, R. A.; Moghaddam, A. B.; Moniri, M.; Ariff, A.; Namvab, F. ZnO-Ag Core Shell Nanocomposite Formed by Green Method Using Essential Oil of Wild Ginger and their Bactericidal and Cytotoxic Effects. *Applied Surface Science*. **2016**, *384*, 517-524.
40. Andrade-Vieira, L. F.; Palmieri, M. J.; Botelho, C. M.; Lubber, J.; Silva, M. F. F. Evaluation of the Antimutagenic Potential of *Psidium Guajava* L. Extracts via Plant Bioassays. *South African Journal of Botany*. **2017**, *113*, 443-448.
41. Weli, A.; Al-Kaabi, A.; Al-Sabahi, J.; Said, S.; Hossain, M. A.; Al-Riyami, S. Chemical Composition and Biological Activities of the Essential Oils of *Psidium Guajava* Leaf. *Journal of King Saud University-Science*. **2019**, *31*, 993-998.
42. Lufuluabo, L. G.; Moke, L. E.; Bongo, G. N.; Liyongo, C. I.; Ashande, C. M.; Sapo, B. S; Mpiana, P. T. A Review on the Phytochemistry and Pharmacology of *Psidium Guajava* L.(Myrtaceae) and Future Direction. *Discovery Phytomedicine*. **2018**, *5*, 7-13.
43. Selvakumar, S. Preliminary Phytochemical Investigation of Various Extracts of Leaves of *Kleinia grandiflora*. *Indo American Journal of Pharmaceutical Research*. **2018**, *8*, 1277-1280.

44. Arunachalam, K. D.; Annamalai, S. K.; Hari, S. One-step Green Synthesis and Characterization of Leaf Extract-mediated Biocompatible Silver and Gold Nanoparticles from *Memecylon Umbellatum*. *International Journal of Nanomedicine*. **2013**, *8*, 1315.
45. de Aquino, A. B.; Cavalcante-Silva, L. H. A.; da Matta, C. B. B.; Epifânio, W. A. D. N.; Aquino, P. G. V.; Santana, A. E. G.; Alexandre-Moreira, M. S.; de Araújo-Júnior, J. X. The Antinociceptive and Anti-Inflammatory Activities of *Aspidosperma Tomentosum* (Apocynaceae). *The Scientific World Journal*. **2013**, *2013*, 1-8.
46. López, P.; Pereboom-de Fauw, D. P.; Mulder, P. P.; Spanjer, M.; de Stoppelaar, J.; Mol, H. G.; de Nijs, M. Straightforward Analytical Method to Determine Opium Alkaloids in Poppy Seeds and Bakery Products. *Food Chemistry*. **2018**, *242*, 443-450.
47. Das, A. J.; Kumar, R.; Goutam, S. P.; Sagar, S. S. Sunlight Irradiation Induced Synthesis of Silver Nanoparticles Using Glycolipid Bio-surfactant and Exploring the Antibacterial Activity. *J Bioeng Biomed Sci*. **2016**, *6*.
48. Shaik, M. R.; Khan, M.; Kuniyil, M.; Al-Warthan, A.; Alkathlan, H. Z.; Siddiqui, M. R. H.; Shaik, J. P.; Ahamed, A.; Mahmood, A.; Khan, M.; Adil, S. F. Plant-Extract-assisted Green Synthesis of Silver Nanoparticles Using *Origanum Vulgare* L. Extract and Their Microbicidal Activities. *Sustainability*. **2018**, *10*, 913.
49. Atarod, M.; Nasrollahzadeh, M.; Sajadi, S. M. Green Synthesis of a Cu/Reduced Graphene Oxide/Fe<sub>3</sub>O<sub>4</sub> Nanocomposite Using *Euphorbia Wallichii* Leaf Extract and its Application as a Recyclable and Heterogeneous Catalyst for the Reduction of 4-nitrophenol and Rhodamine B. *RSC Advances*. **2015**, *5*, 91532–91543.
50. Diantariani, N. P.; Wahyuni, E. T.; Kartini, I.; Kuncaka, A. Ag/ZnO Photocatalyst for Photodegradation of Methylene Blue. *Materials Science and Engineering*. **2019**, *509*, 012099.
51. Sriram, T.; Pandidurai, V. Synthesis of Silver Nanoparticles from Leaf Extract of *Psidium Guajava* and its Antibacterial Activity Against Pathogens. *International Journal of Current Microbiology and Applied Sciences*. **2014**, *3*, 146-152.

52. Abboud, Y.; Eddahbi, A.; El Bouari, A.; Aitenneite, H.; Brouzi, K.; Mouslim, J. Microwave-Assisted Approach for Rapid and Green Phytosynthesis of Silver Nanoparticles Using Aqueous Onion (*Allium Cepa*) Extract and Their Antibacterial Activity. *Journal of Nanostructure in Chemistry*. **2013**, *3*, 1-7.
53. Fahlman, D. B. *Materials Chemistry*, Springer, Dordrecht: The Netherlands, 2007, 1-488.
54. Fesenk, O.; Yatsenko, L. *Nanochemistry, Biotechnology, Nanomaterials, and Their Applications*; Springer Proceedings in Physics (214): Chernivtsi, 2017.
55. Choi, Y. I., Jung, H. J., Shin, W. G., & Sohn, Y. Band Gap-engineered ZnO and Ag-ZnO by Ball-milling Method and Their Photocatalytic and Fenton-like Photocatalytic Activities. *Applied Surface Science*. **2015**, *356*, 615-625.
56. Burlibaşa, L.; Chifiriuc, M. C.; Lungu, M. V.; Lungulescu, E. M.; Mitrea, S.; Sbarcea, G.; Popa, M.; Maşrut,escu, L.; Constantin, N.; Bleotu, C.; Hermenean, A. Synthesis, Physico-chemical Characterization, Antimicrobial Activity and Toxicological Features of Ag-ZnO Nanoparticles. *Arabian Journal of Chemistry*. **2020**, *13*, 4180-4197.
57. Dou, P.; Tan, F.; Wang, W.; Sarreshteh, A.; Qiao, X.; Qiu, X.; Chen, J. One-step Microwave-assisted Synthesis of Ag-ZnO/Graphene Nanocomposites with Enhanced Photocatalytic Activity. *Journal of Photochemistry and Photobiology A: Chemistry*. **2015**, *302*, 17-22.
58. Conduction and Valence Band Diagram: <https://electronicscoach.com/wp-content/uploads/2017/07/Energy-Band-Gap-Diagram.jpg/>  
<https://electronicscoach.com/material.html> (Accessed on 11 March, 2020).
59. Singh, R.; Barman, P. B.; Sharma, D. Synthesis, Structural and Optical Properties of Ag Doped ZnO Nanoparticles with Enhanced Photocatalytic Properties by Photo Degradation of Organic Dyes. *Journal of Materials Science: Materials in Electronics*. **2017**, *28*, 5705-5717.
60. Muñoz-Fernandez, L.; Sierra-Fernández, A.; Milošević, O.; Rabanal, M. E. Solvothermal Synthesis of Ag-ZnO and Pt/ZnO Nanocomposites and Comparison of Their Photocatalytic Behaviors on Dyes Degradation. *Advanced Powder Technology*. **2016**, *27*, 983-993.



61. Bouzid, H.; Faisal, M.; Harraz, A. F.; Al-Sayari, A. S.; Ismail, A. A. Synthesis of Mesoporous Ag-ZnO Nanocrystals with Enhanced Photocatalytic Activity. *Catalysis Today*. **2015**, 252, 20-26.
62. Wang, X. Q.; Han, S. F.; Zhang, Q. W.; Zhang, N.; Zhao, D. D. Photocatalytic Oxidation Degradation Mechanism Study of Methylene Blue Dye Waste Water with GR/iTO<sub>2</sub>. In *Matec Web of Conferences*. **2018**, 238, p. 03006. EDP Sciences.
63. Mathew, J. J.; Vazhacharickal, J. P.; Sajeshkumar, N. K.; Joy, K. J. Phytochemical Analysis and Invitro Hemostatic Activity of Mimosa Pudica, Hemigraphis Colorata And Chromolaena Odorata Leaf Extracts. *CIBTech Journal of Pharmaceutical Sciences*. **2016**, 5, 16-34.
64. Gupta, M.; Tomar, R. S.; Kaushik, S.; Mishra, R. K.; Sharma, D. Effective Antimicrobial Activity of Green ZnO Nanoparticles of *Catharanthus Roseus*. *Frontiers in Microbiology*. **2018**, 9, 2030.
65. Jamdagni, P.; Khatri, P.; Rana, J. S. Green Synthesis of Zinc Oxide Nanoparticles Using Flower Extract of Nyctanthes Arbor-tristis and Their Antifungal Activity. *Journal of King Saud University-Science*. **2018**, 30, 168-175.
66. Begum, N.; MH, M. I.; Mathew, S.; Govindaraju, A.; Qadri, I. Green Synthesis, Antioxidant Potential and Hypoglycemic Effect of Silver Nanoparticles Using Ethanolic Leaf Extract of *Clausena Anisata* (Willd.) Hook. F. Ex Benth. of Rutaceae. *Pharmacognosy Journal*. **2016**, 8, 565-575.
67. Essawy, A. A. Silver Imprinted Zinc Oxide Nanoparticles: Green Synthetic Approach, Characterization and Efficient Sunlight-induced Photocatalytic Water Detoxification. *Journal of Cleaner Production*. **2018**, 183, 1011-1020.
68. Sohrabnezhad, S.; Seifi, A. The Green Synthesis of Ag/ZnO in Montmorillonite with Enhanced Photocatalytic Activity. *Applied Surface Science*, **2016**, 386, 33-40.
69. Chamjangali, M. A.; Bagherian, G.; Javid, A.; Boroumand, S.; Farzaneh, N. Synthesis of Ag-ZnO with Multiple Rods (Multipods) Morphology and its Application in the Simultaneous Photocatalytic Degradation of Methyl Orange and Methylene

Blue. *Spectrochimica Acta Part A: Molecular and Biomolecular Spectroscop.* **2015**, *150*, 230-237.

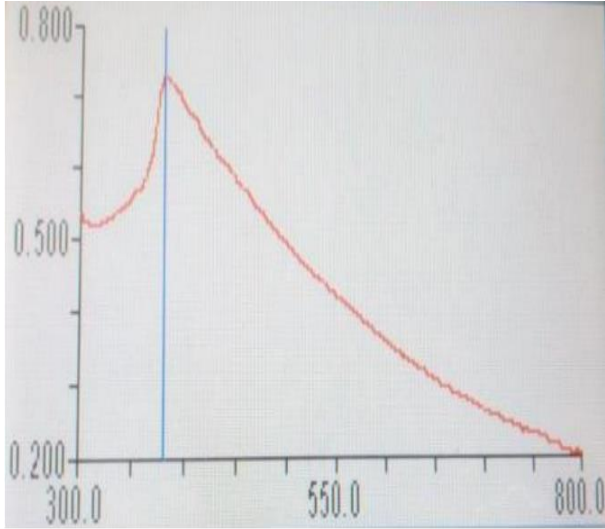
70. Nagaraju, G.; Udayabhanu; Shivaraj; Prashanth, A. S.; Shastri, M.; Yathish, V. K.; Anupama, C.; Rangappa, D. Electrochemical Heavy Metal Detection, Photocatalytic, Photoluminescence, Biodiesel Production and Antibacterial Activities of Ag-ZnO Nanomaterial. *Materials Research Bulletin.* **2017**, *94*, 54-63.
71. Iyanuloluwa, O.; Adamu, K. Y.; Audu, J. A. Antibacterial and Antifungal Activities of Aqueous Leaves Extract of Some Medicinal Plants. *GSC Biological and Pharmaceutical Sciences.* **2019**, *9*, 062-069.
72. Biswas, B.; Rogers, K.; McLaughlin, F.; Daniels, D., Yadav, A. Antimicrobial Activities of Leaf Extracts of *Guava (Psidium Guajava L.)* on Two Gram-negative and Gram-positive Bacteria. *International Journal of Microbiology.* 2013, *2013*, 1-7.
73. Hosseini, S. M.; Sarsari, I. A.; Kameli, P.; Salamati, H. Effect of Ag Doping on Structural, Optical, and Photocatalytic Properties of ZnO Nanoparticles. *Journal of Alloys and Compounds.* **2015**, *640*, 408-415.
74. Rajaboopathi, S.; Thambidurai, S. Enhanced Photocatalytic Activity of Ag-ZnO Nanoparticles Synthesized by Using *Padina Gymnospora* Seaweed Extract. *Journal of Molecular Liquids.* **2018**, *262*, 148-160.
75. Getie, S.; Belay, A.; Chandra Reddy, A. R.; Belay, Z. Synthesis and Characterizations of Zinc Oxide Nanoparticles for Antibacterial Applications. *Journal of Nanomedicine and Nanotechnology.* **2017**, *8*, 1-8.
76. Somchaidee, P.; Tedsree, K. Green Synthesis of High Dispersion and Narrow Size Distribution of Zero-valent Iron Nanoparticles Using *Guava Leaf (Psidium Guajava L)* Extract. *Advances in Natural Sciences: Nanoscience and Nanotechnology.* **2018**, *9*, 035006.
77. Sharmila, C.; Ranjith Kumar, R.; Chandar Shekar, B. *Psidium Guajava*: A Novel Plant in the Synthesis of Silver Nanoparticles for Biomedical Applications. *Asian Journal of Pharmaceutical and Clinical Research.* **2018**, *11*, 341-345.

78. Ajayi, E.; Afolayan, A. Green Synthesis, Characterization and Biological Activities of Silver Nanoparticles from Alkalinized Cymbopogon Citratus Stapf. *Advances in Natural Sciences: Nanoscience and Nanotechnology*. **2017**, *8*, 015017.
79. Costa, G. G.; Brito, C. C.; Terezo, A. J.; Cardoso, A. P.; Ionashiro, E. Y.; B de Siqueira, A. Preparation, Characterization and Antioxidant Evaluation of Cu (II) and Zn (II) Tannates. *The Open Chemistry Journal*. **2018**, *5*, 158-171.
80. Manikandan, V. S.; Palai, A. K.; Mohanty, S.; Nayak, S. K. Surface Plasmonic Effect of Ag Enfold ZnO Pyramid Nanostructured Photoanode for Enhanced Dye Sensitized Solar Cell Application. *Ceramics International*. **2018**, *44*, 21314-21322.
81. Jayarambabu, N.; Rao, K. V.; Rajendar, V. Biogenic Synthesis, Characterization, Acute Oral Toxicity Studies of Synthesized Ag and ZnO Nanoparticles Using Aqueous Extract of Lawsonia Inermis. *Materials Letters*. **2018**, *211*, 43-47.
82. Alshamsi, H. A. H.; Hussein, B. S. Hydrothermal Preparation of Silver Doping Zinc Oxide Nanoparticles: Study the Characterization and Photocatalytic Activity. *Oriental Journal of Chemistry*. **2018**, *34*, 1898-1907.
83. Fakhari, S.; Jamzad, M.; Fard, K. H. Green Synthesis of Zinc Oxide Nanoparticles: a Comparison. *Green Chemistry Letters and Reviews*. **2019**, *12*, 19-24.
84. Pavithra, K. S.; Yashoda, M. P.; Prasannakumar, S. Effect of Microwave Irradiation Power for the Morphological Changes of ZnO Nanoparticles. In *IOP Conference Series: Materials Science and Engineering*. **2019**, *577*, p. 012120. IOP Publishing.
85. Bakatula, E. N.; Richard, D.; Neculita, C. M.; Zagury, G. J. Determination of Point of Zero Charge of Natural Organic Materials. *Environmental Science and Pollution Research*. **2018**, *25*, 7823-7833.
86. Kosmulski, M. The pH Dependent Surface Charging and Points of Zero Charge. VI. Update. *Journal of Colloid and Interface Science*. **2014**, *426*, 209-212.

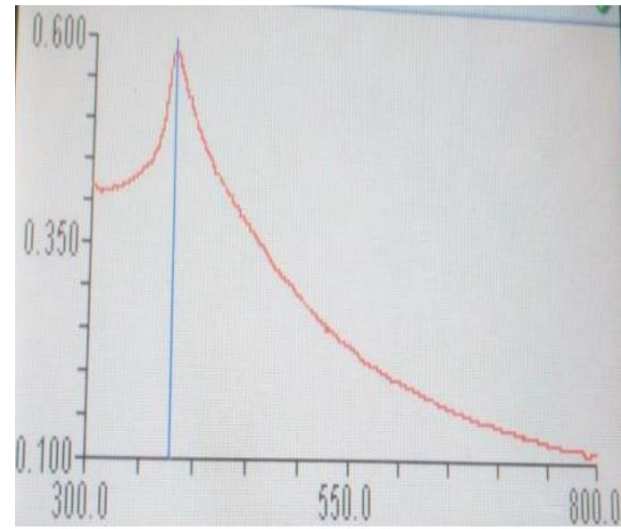
87. Mendoza-Mendoza, E.; Nuñez-Briones, A. G.; García-Cerda, L. A.; Peralta-Rodríguez, R. D.; Montes-Luna, A. J. One-step Synthesis of ZnO and Ag/ZnO Heterostructures and Their Photocatalytic Activity. *Ceramics International*. **2018**, *44*, 6176-6180.
88. Dong, B.; Yu, X.; Dong, Z.; Yang, X.; Wu, Y. Facile Synthesis of ZnO Nanoparticles for the Photocatalytic Degradation of Methylene Blue. *Journal of Sol-Gel Science and Technology*. **2017**, *82*, 167-176.
89. Bozetine, H.; Wang, Q.; Barras, A.; Li, M.; Hadjersi, T.; Szunerits, S.; Boukherroub, R. Green Chemistry Approach for the Synthesis of ZnO–carbon Dots Nanocomposites With Good Photocatalytic Properties Under Visible Light. *Journal of Colloid and Interface Science*. **2016**, *465*, 286-294.
90. El-Bindary, A. A.; Ismail, A.; Eladl, E. F. Photocatalytic Degradation of Reactive Blue 21 Using Ag Doped ZnO Nanoparticles. *Journal of Materials and Environmental Science*. **2019**, *10*, 1258-1271.

## Appendix A

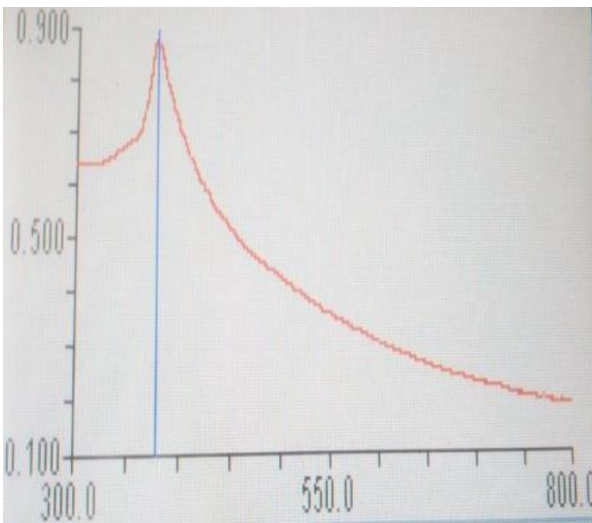
Absorbance peak of Ag-ZnO NCs at differne pH values.



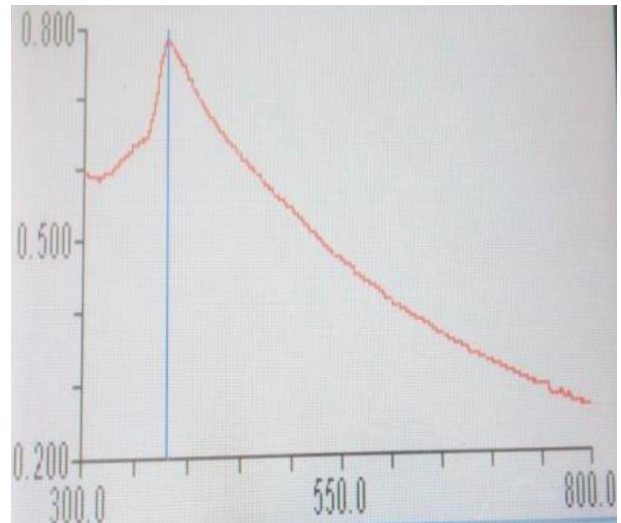
A1: Absorbance peak of Ag-ZnO NCs (pH = 6),  $\lambda_{\text{max}} = 380.7 \text{ nm}$



A2: Absorbance peak of Ag-ZnO NCs (pH = 8),  $\lambda_{\text{max}} = 378.8 \text{ nm}$



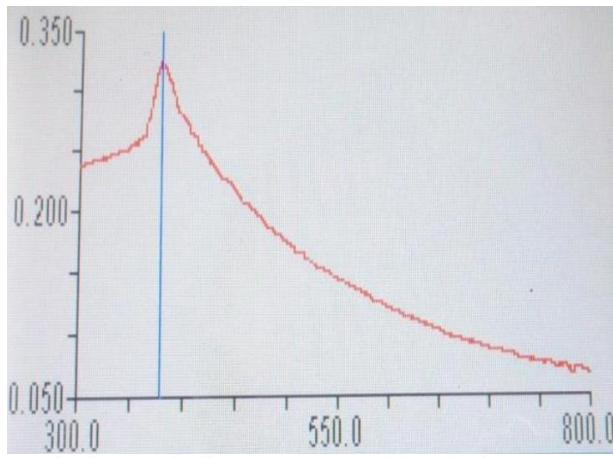
A3: Absorbance peak of Ag-ZnO NCs (pH = 9),  $\lambda_{\text{max}} = 378.8 \text{ nm}$



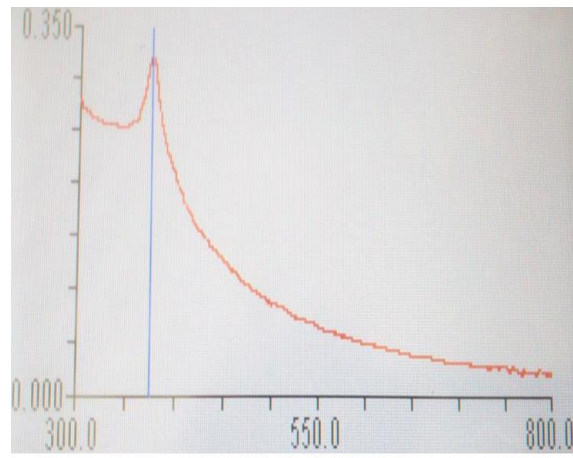
A4: Absorbance peak of Ag-ZnO NCs (pH = 10),  $\lambda_{\text{max}} = 380.7 \text{ nm}$

## Appendix B

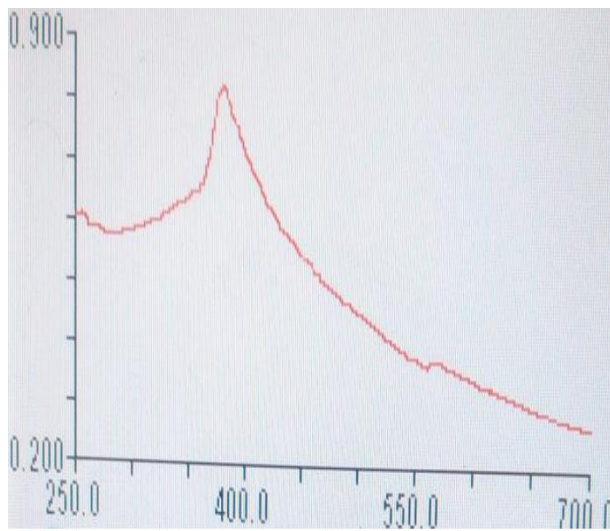
Absorbance peak of Ag-ZnO NCs at different dopant concentrations.



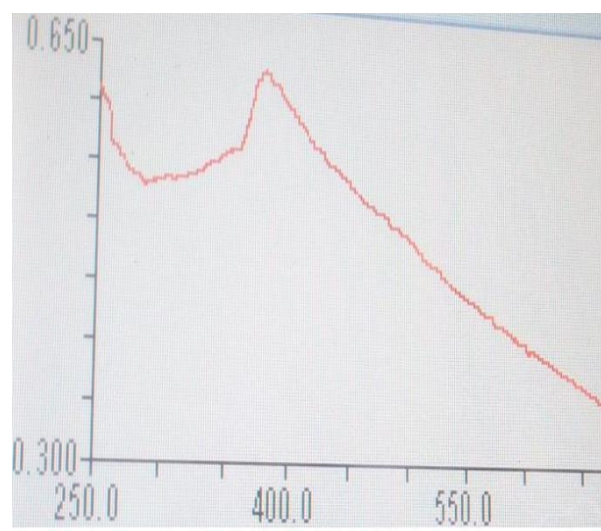
B<sub>1</sub>: Absorbance peak of Ag-ZnO NCs (0.13% AgNO<sub>3</sub>),  $\lambda_{\text{max}} = 378.8$  nm



B<sub>2</sub>: Absorbance peak of Ag-ZnO NCs (0.25% AgNO<sub>3</sub>),  $\lambda_{\text{max}} = 375.0$  nm



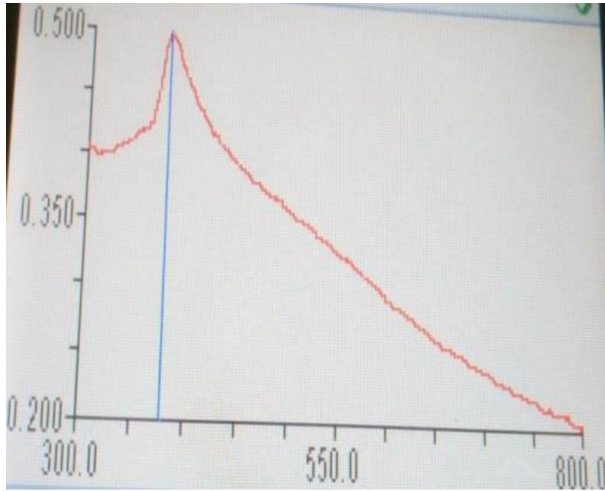
B<sub>3</sub>: Absorbance peak of Ag-ZnO NCs (0.5% AgNO<sub>3</sub> dopant),  $\lambda_{\text{max}} = 380.3$  nm



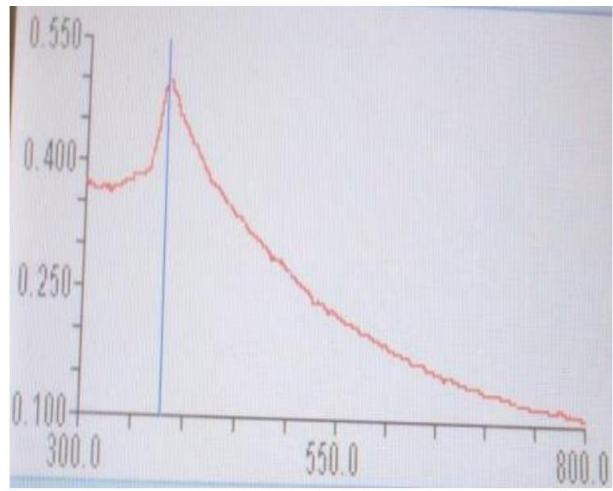
B<sub>4</sub>: Absorbance peak of Ag-ZnO NCs (1% AgNO<sub>3</sub> dopant),  $\lambda_{\text{max}} = 382.1$  nm

## Appendix C

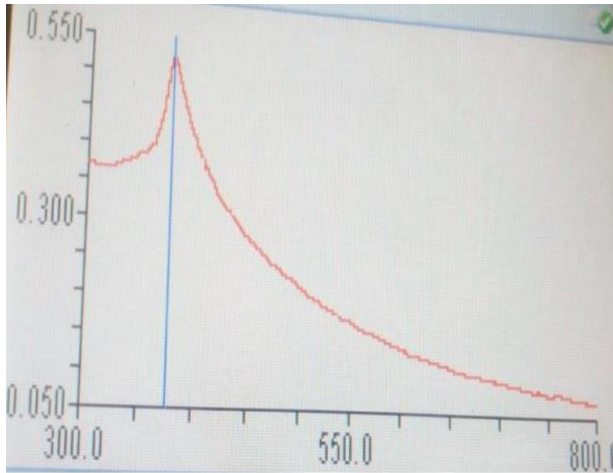
Effect of concentration of *Guava* leaf extract on Ag-ZnO NCs synthesis.



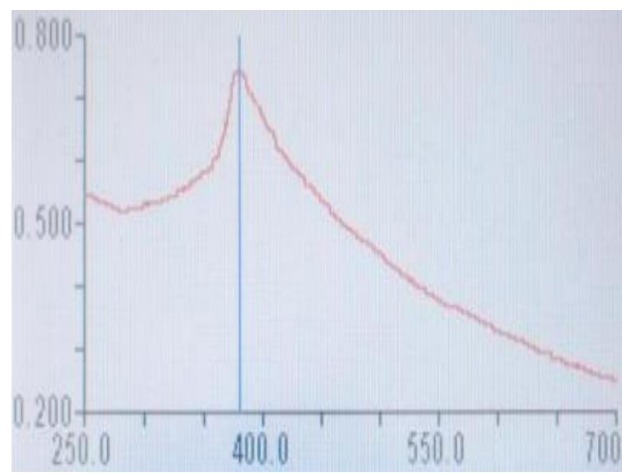
C1: Absorbance peak of Ag-ZnO NCs (3 mL *Guava* extract),  $\lambda_{\max} = 378.8$  nm



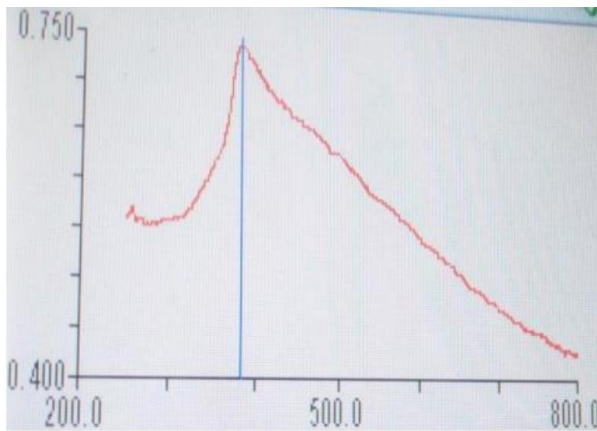
C2: Absorbance peak of Ag-ZnO NCs (5 mL *Guava* extract),  $\lambda_{\max} = 378.8$  nm



C3: Absorbance peak of Ag-ZnO NCs (7 mL *Guava* extract),  $\lambda_{\max} = 376.9$  nm



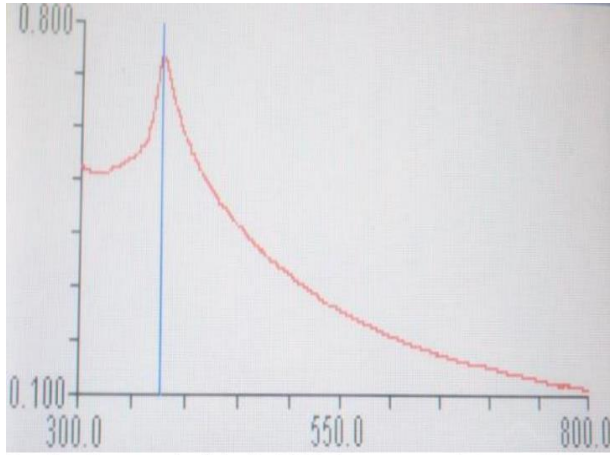
C4: Absorbance peak of Ag-ZnO NCs (9 mL *Guava* extract),  $\lambda_{\max} = 380.3$  nm



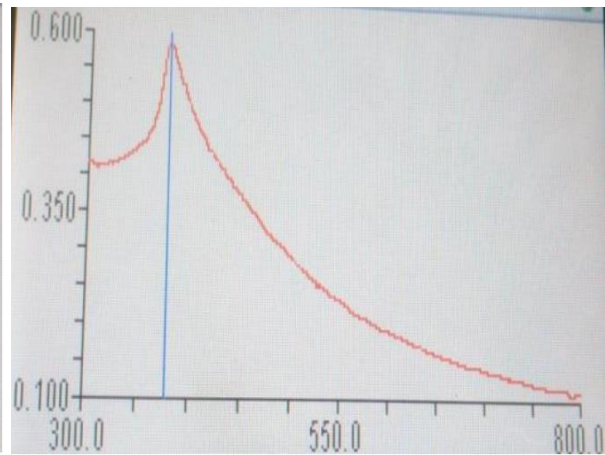
C5: Absorbance peak of Ag-ZnO NCs (11 mL *Guava* extract),  $\lambda_{\max} = 382.7$  nm

## Appendix D

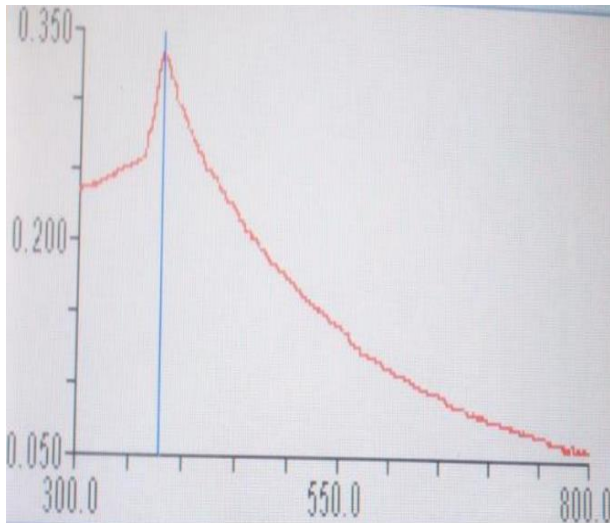
Temperature effects on synthesis of Ag-ZnO NCs.



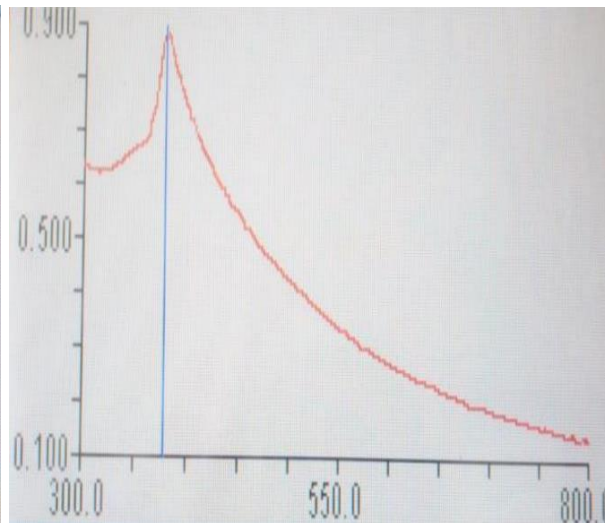
D1: Absorbance peak of Ag-ZnO NCs (at room temp.),  $\lambda_{\text{max}} = 376.9$  nm



D2: Absorbance peak of Ag-ZnO NCs (35 oC),  $\lambda_{\text{max}} = 378.8$  nm



D3: Absorbance peak of Ag-ZnO NCs (55 oC),  $\lambda_{\text{max}} = 378.8$  nm

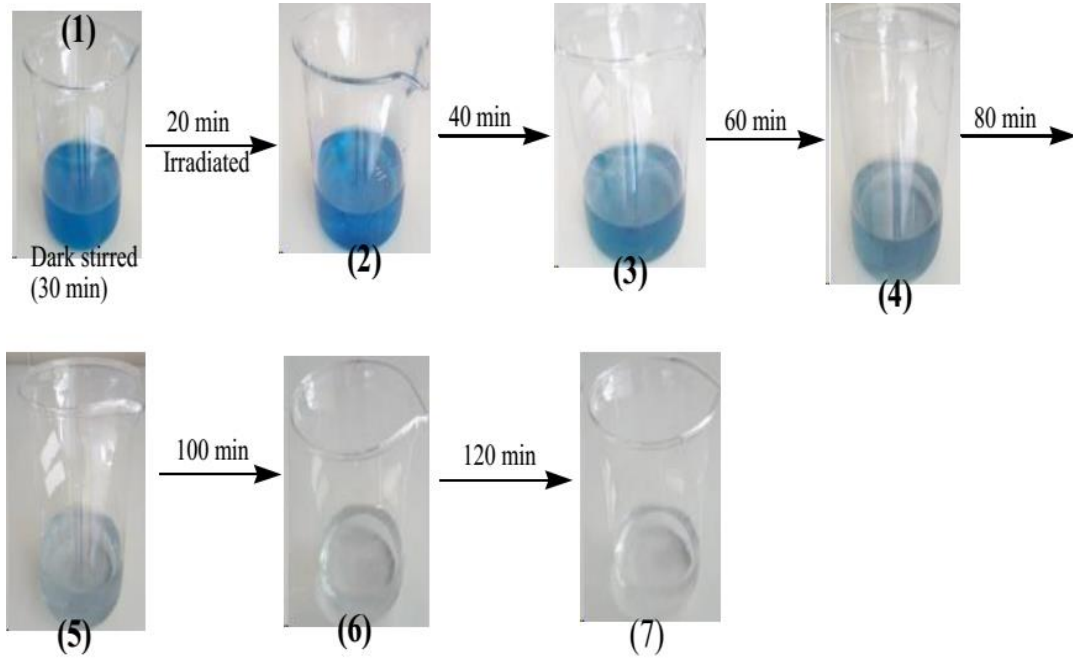


D4: Absorbance peak of Ag-ZnO NCs (75 oC),  $\lambda_{\text{max}} = 378.8$  nm

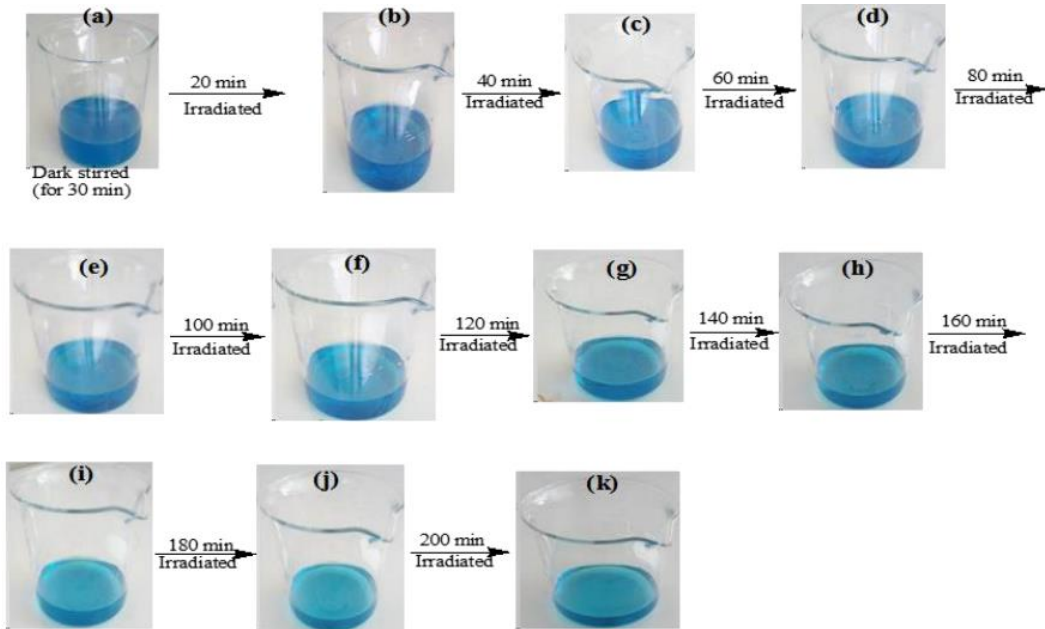


## Appendix E

Photocatalytic degradation and decolorization of methylene blue (MB) dye:



E<sub>1</sub>: Decolorization of MB dye catalyzed by Ag-ZnO NCs.



E<sub>2</sub>: Decolorization of MB dye catalyzed by natural sunlight.